Comparison of Eemian and Holocene sea surface temperatures in the Bering Sea including terminations II and I

Master Thesis MSc Programme Marine Geosciences
Department of Geosciences
University of Bremen

by

Lukas Belz
Bremen, 2013

Table of contents

Abstract

The global mean temperature during the Eemian interglacial (ca. 130-115 ka BP) was about 2°C warmer than today and is thought to have had a climate condition comparable to conditions, which might occur due to modern anthropogenic climate change. Paleoceanographic records from the sub-arctic Pacific and especially the Bering Sea over this important period are very limited. Reconstruction of sea surface temperatures (SST) can lead to assumptions about processes of climate change and help indicate changes to environmental conditions. This thesis contains new alkenone derived SSTs and qualitative IP_{25} sea ice reconstructions, over glacial termination II and marine isotope stage 5 (MIS5) from the Western Bering Sea (core SO201-2-85KL). The results were compared to Holocene records from the same area, as well as to records over MIS5 and the Holocene from North Pacific and North Atlantic. The SST record over glacial termination II and the Eemian period shows many parallels to the climate development and temperature variability in the Bering Sea during the last 15 ka. In contrast to Atlantic and Pacific temperatures, the SST over the last interglacial was not enhanced compared to the Holocene thermal maximum. This suggests a cooling factor within the Eemian Bering Sea, which possibly includes changes in regards of currents or atmospheric interaction between the Bering Sea and the North Pacific as well as to teleconnections to the North Atlantic.

1. Introduction

The aim of this master thesis will be to compare existing Holocene sea surface temperature (SST) records from the Bering Sea with new alkenone-based SST-data from the Eemian period (the last interglacial, ca. 130-115 ka before present (BP)). Hereby a focus shall also be laid on glacial termination II and I, the preceding deglaciation phases of the Eemian and the Holocene respectively. Additionally IP_{25}, a biomarker for sea ice occurrence, shall be taken into account regarding deglaciation periods and sea ice dynamics. To put the Eemian SST values into supra-regional context, they shall also be compared to other Temperature records from North Pacific and North Atlantic.

The SST measurements done in this Thesis are embedded in topic 8 of the REKLIM climate initiative. This initiative focuses on regional climate variability (REgionale KLIMaänderungen) and supra-regional interactions and is funded by the Helmholtz research community. Topic 8 of this initiative deals with rapid climate change derived from proxy data. As the results of this thesis are used for this initiative, its motivation is also a part of the motivation of this thesis. However, hypotheses which are related to this motivation cannot be tested by the results of this thesis alone, but of the results of several studies.

Motivation & scientific questions

During the Eemian interglacial orbital configurations were comparable to today, but with higher summer insolation maxima in the northern hemisphere, leading to similar temperature trends with higher magnitudes (Leduc et al., 2010). This makes the Eemian interesting for comparison of long term climate trends with the Holocene. The trends should be similar, but due to higher magnitudes they should be more distinctive during Eemian times. During the Eemian the global mean temperature was about 2°C higher than today (Otto-Bliesner et al., 2006; Kopp et al., 2009). The Eemian is therefore of special interest. Although it is not a complete analogue to the climate situation that may occur if the 2°C limit is crossed, consequences, like global sea level rise, can be comparable (Rohling et al., 2008). This limit is defined by the United Nations Framework Convention on Climate Change (UNFCCC), in order to avoid dangerous climate change (EU Climate Change Expert Group 'EG Science', 2008). A very important aspect regarding this is that during the Eemian the global mean sea level, reconstructed with proxy data, was at least 6 m higher than today (Kopp et al., 2009). The common explanation is that melting of continental ice sheets led to a higher sea level. Climate models suggest, that no more than 3.4 m were contributed by the Greenland ice sheet (GIS), which is also supported with arctic paleoclimatic data (Otto-Bliesner et al., 2006). More recent data from a new Greenland ice core, the first from Greenland to cover the complete Eemian, favours models with a contribution of about 2 m (NEEM Community Members, 2013). A probable source for the water, which contributed to the additional rise of 2.6-4 m sea level, would be a destabilization of the West Antarctic ice sheet (WAIS) (Overpeck et al., 2006). As the Eemian may have had a similar climate situation, as developed by anthropogenic global warming, it is of high importance to check these models against global proxy data, to search for any evidence, which could determine if this scenario may be realistic.

The amount of published SST-proxy data for the sub polar North Pacific and its marginal seas is small, although there has been some improvement over the last few years (e.g. Ternois et al., 2000; Kiefer & Kienast, 2005). Still this area lacks on data over longer terms. In the Bering Sea, there are five alkenone datasets available, none of them yet has a record reaching longer than the last glacial maximum (LGM) (Max et al., 2012; Caissie et al., 2010). There is no Eemian SST-data in the Bering Sea available yet, so this thesis will fill a gap in the data records in order for a better oceanographic understanding regarding the Bering Sea and its interactions with the North Pacific.

Another key motivation is the understanding of climate interaction between North Atlantic and North Pacific. Kim et al. (2004) suggested a temperature seesaw between these two climatic realms, based on late Holocene climate models and several proxy records from this period, which showed rising temperatures in the North Pacific and decreasing temperatures in the North Atlantic. This seesaw is thought to be driven by an atmospheric teleconnection between the North Atlantic Oscillation (NAO), and the Pacific-North America Oscillation (PNA). A high NAO index, referring to a high pressure gradient between an Iceland low and an Acores high, would therefore correspond to a PNA low and vice versa. Leduc et al. (2010) enhanced the GHOST database used by Kim et al. (2004) which included supporting data in the North Atlantic and mid-latitude North Pacific. However, recent Holocene SST data from the subarctic Pacific and its marginal seas stand in contradiction to this theory and describe parallel patterns between North Atlantic and subarctic Pacific during glacial termination I and the Holocene (Max et al., 2012). Recent modelling suggests that an Atlantic-Pacific seesaw is related to meridional overturning circulation and only exists when the Bering Strait is closed (Hu et al., 2012). Comparison of Eemian SST temperatures from the North Atlantic and the subarctic Pacific can show temperature teleconnections between both realms on a longer scale. The Eemian period featured higher insolation values, leading to higher amplitudes in climate signals. Therefore, the character of such a teleconnection might also be easier to identify.

The motivation, results in the following three general scientific questions:

- Did the higher insolation during the Eemian interglacial lead to significant changes regarding interglacial SST trends?

- How do glacial termination I and II compare, regarding SST and sea ice development?

- Is there a relation between North Atlantic and North Pacific temperatures trends during glacial termination II and the Eemian interglacial?

2. Geographic setting

2.1. Current regime within the Bering Sea and its connection to adjacent areas

The surface circulation of the Bering Sea is dominated by a cyclonic gyre. It's boundaries are, as shown in **Figure 1**, the Kamchatka current to the west, the Bering Sea slope current to the north east and the Aleutian north slope current to the south. Within this gyre is a northward flowing current, which enters the Bering Sea at Near Strait and joins the Kamchatka current at the northern edge of the Shirshov Ridge (Takahashi, 2005; Stabeno et al., 1999).
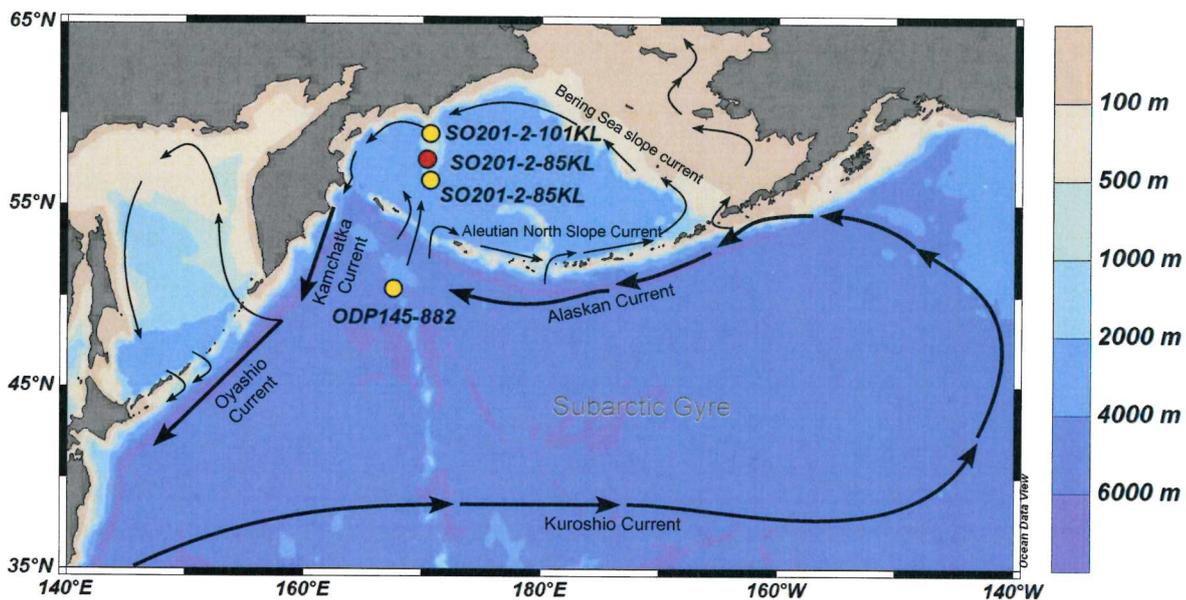
Figure 1: Current system in the modern Bering Sea and sub arctic North Pacific

The red circle indicates the location of the core analysed in this thesis, yellow circles show core locations of SST records from other studies, which were used for comparison in this thesis. Arrows show a schematic of the current regime, based on Stabeno et al. (1999). Bathymetric map was created using "Ocean Data View" (Schlitzer, 2012).

Gateways and interactions with adjacent areas

The Bering Sea is connected to the Pacific via few passages between the Aleutians. The most important gateways are the Unimak Passage to the east, the Amchitka Passage to the South and Kamchatka, and Near Strait to the West. Apart of the two western straits, the passages are rather shallow, which led to changes of current patterns during glacials. **Figure 2** outlines modern flow volumes through the southern passages. The cold water mass passing through Kamchatka Strait contributes to the Eastern Kamchatka-Oyashio-current system, which is heading southward. These currents represent the western boundary of the North Pacific sub-

arctic gyre. Along the southern side of the Aleutian Islands flows the Alaskan current, which is the northern edge of the subarctic gyre.
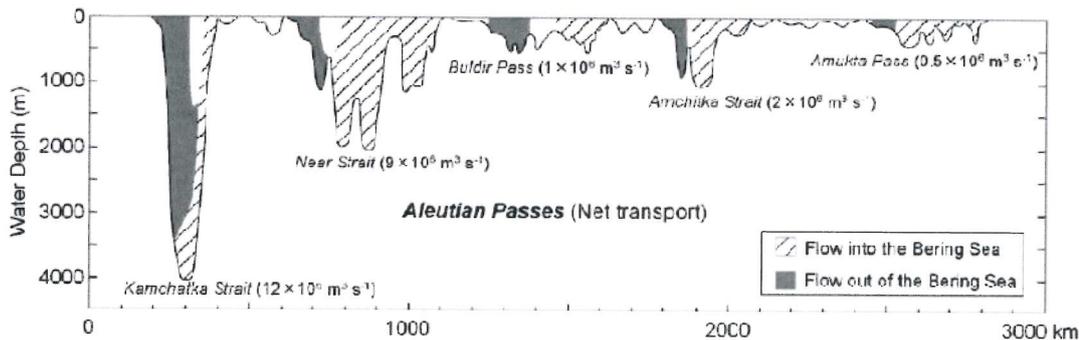
Figure 2: Profile of flows between Pacific and Bering Sea

Source: Takahashi (2005).

During interglacials there is also a connection to the Arctic Ocean via the Bering Strait, which is rather small but important regarding the global conveyor belt. The Bering Strait transports surface water, with a relative low salinity, from the Bering Sea to the more saline Arctic Ocean (Stabeno et al., 1999).

As stated in the motivation, models suggest a seesaw regarding thermo-haline circulation in glacials. The glacial closure of the Bering Strait is thought to have disturbed the Atlantic meridional overturning circulation (AMOC). This led to a cooler North Atlantic, but enhanced a production of North Pacific intermediate water (NPIW) and created a Pacific meridional overturning circulation (PMOC) (Hu et al., 2012). Recent neodymium isotope data brought evidence for NPIW activity during early MIS 5d and the western Bering Sea is thought to be a source region (Horikawa et al., 2010).

The glacial sea level drops led also to an exposure of the eastern shelf area and affected the capacity of gateways between the eastern Aleuts and therefore decrease the incoming amount of water so that the slope current is weakened (Tanaka & Takahashi, 2005).

2.2. Modern surface temperatures and sea ice condition

Figure 3 gives an overview about the distribution of September and March surface temperatures in the North Pacific in 2009. During late summer there is a northward directed temperature gradient until latitudes of 45° N. Further to the North, the temperature distribution is influenced by the Aleutian Island, which leads to lower temperatures in the Bering Sea, compared to the sea of Okhotsk, which lies at the same latitude.
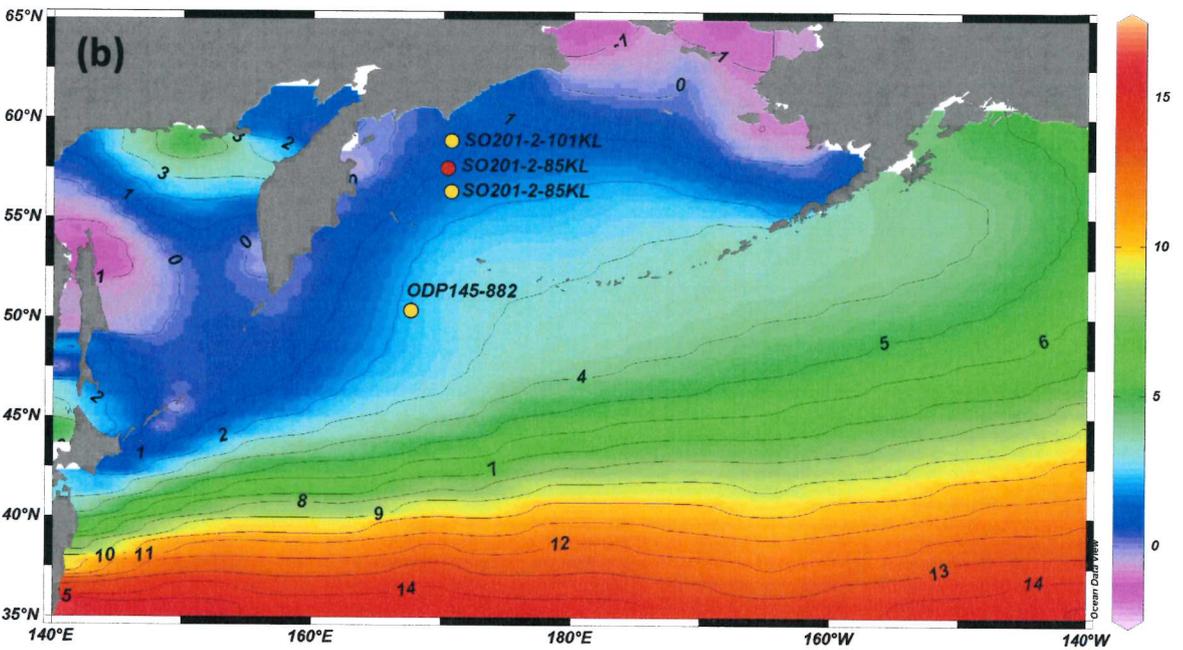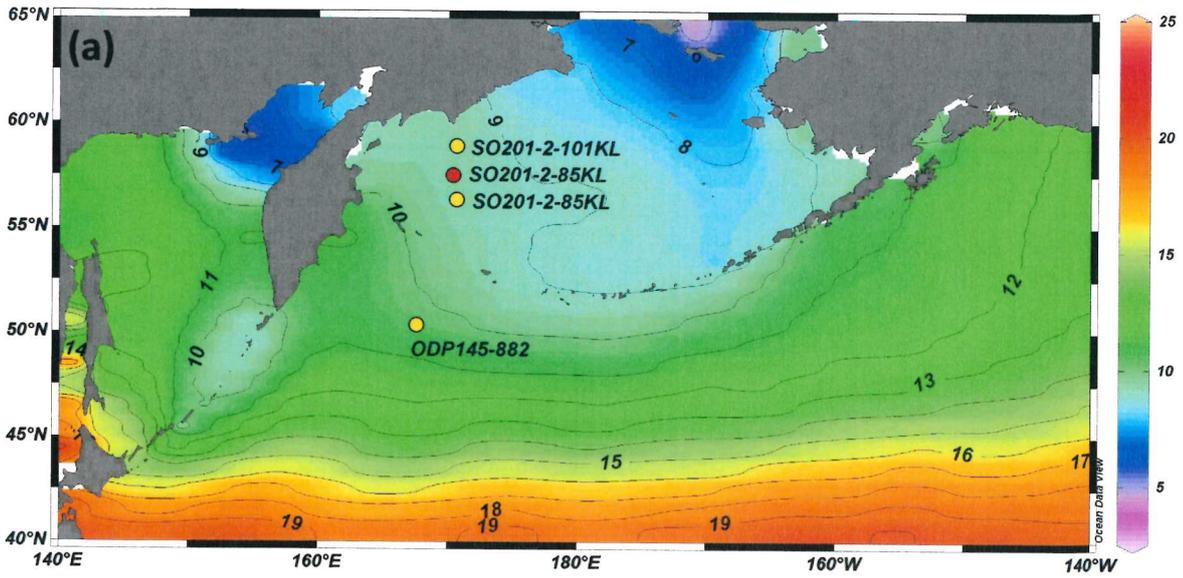
Figure 3: Sea surface temperature distribution in the Bering Sea and subarctic North Pacific in 2009

The surface color indicates (a) September and (b) March SST. Data source: Locarni et al. (2010). Map was created using "Ocean Data View" (Schlitzer, 2012).

In March the latitude parallel temperature distribution is shifted southward. North of 40° the gradient is turning anti clockwise, leading to cold temperatures to the west and slightly warmer surface water to the east. This gradient intensifies towards north, leading to a temperature difference above 5°C at 50° N, with very cold temperatures east of Kamchatka. In

the Bering Sea this temperature pattern is weakened and north of 57° the SST distribution is latitude parallel.

These great inner annual SST dynamics in the subarctic pacific regarding SST are strongly coupled to the Aleutian low pressure system, which is influenced by PNA and two other important oscillations, the Pacific Decadal Oscillation (PDO), and the El Nino Southern Oscillation (ENSO) (Max et al., 2012; Niebauer, 1988). During winter the climate is dominated by the pressure gradient between the Siberian high and the Aleutian low pressure system. This leads to strong northerly winds and three to five storms per month, which transport cold air masses from the arctic southward. l Nino events lead to a weakened Aleutian Low, which is moved south east, and leads to warmer temperatures in the Bering Sea. In summer the Aleutian Low is rather weak, leading to slow winds, which favours insolation as main driver for summer climate (Niebauer et al., 1999).

Today, during end of winter, sea ice coverage in the Bering Sea reaches its maximum extension, as depicted in **Figure 4**, in the shelf area to the east and the coastal regions to the northwest (Niebauer et al., 1999). Apart of the coastal regions, the western Bering Sea is ice free throughout the year.
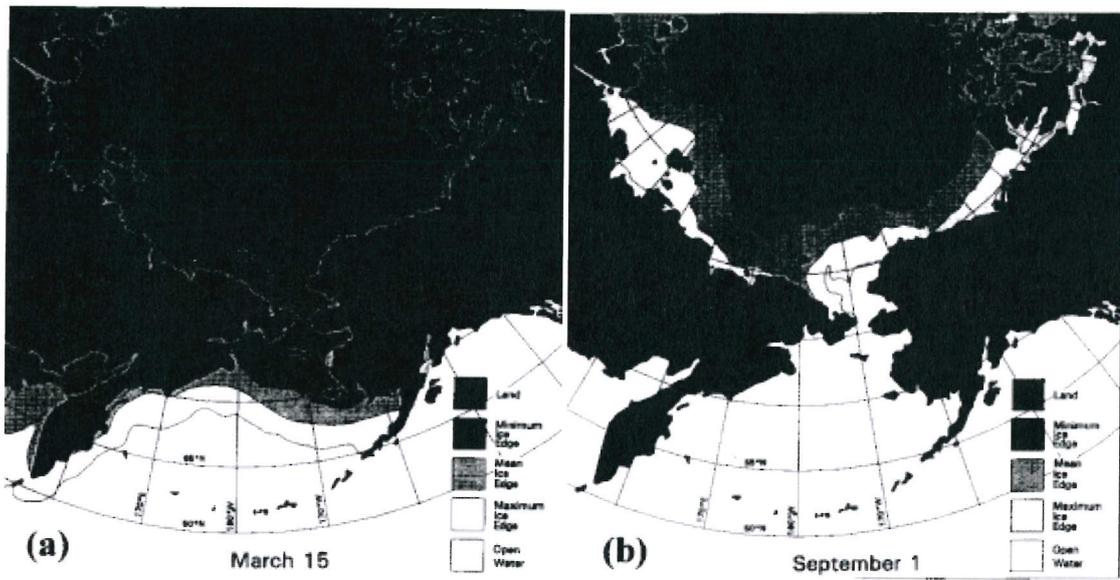
Figure 4: Sea ice distribution variability in the Bering Sea

Ice extension is depicted during (a) summer and (b) winter (Niebauer et al., 1999).

2.3. Eemian climate in the subarctic

In many publications the Eemian and marine isotope stage 5e (MIS 5e) are used as synonyms for the last interglacial (e.g. Rohling et al., 2007; NEEM Community Members, 2013). However there are publications, using divergent definitions for both terms. MIS 5e is coupled to global marine oxygen isotope stacks, while the Eemian sequences originally refer to changes regarding European vegetation zones. Both intervals overlap mostly, but the base of MIS 5e is ca. 5 ka older than the Eemian, which does reach well into MIS 5d (Shackelton et al., 2003; Kukla et al., 2002). In this thesis both terms shall refer to the last interglacial and characterize the time span between 130 and 115 ka BP.

As mentioned above, the last interglacial had a higher global mean temperature than today. To focus on the northern North Pacific, **Figure 5** compares MIS 5e and Holocene June insolation at 60°N. Both curves describe a peak with about the same width, but differ in peak intensity. Eemian insolation is more than 20 W/m² increased. Another major difference is the end of the warm period. Whereas the Holocene ends in an insolation state, which is a bit higher than before the Holocene, the insolation after MIS 5e displays a large drop. As the Eemian peak insolation is also stronger, while the period length is about the same, the increasing trend towards the peak and the descending afterwards is clearly steeper during the Eemian.
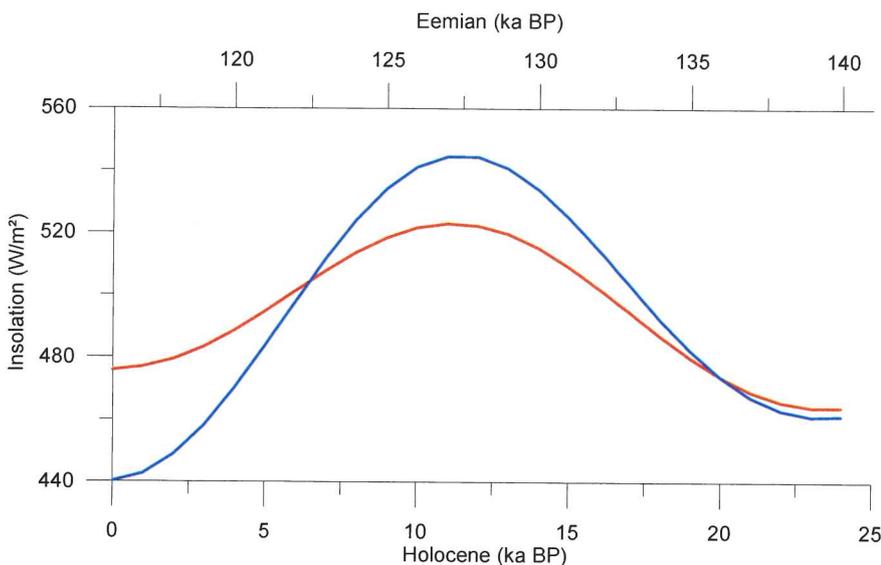
Figure 5: Eemian and Holocene June insolation

Insolation at 60°N is plotted against time. The red line indicates the Holocene insolation and is related to the axis at the bottom of the graph. The blue line indicates the Eemian insolation and is related to the axis on the top of the graph. Data source: Berger & Loutre (1991).

Whereas the global mean temperature during the Eemian maxima was enhanced by 2°C, the northern high latitudes were even warmer, due to amplification. This amplification takes place through positive feedbacks, like for example ice-albedo feedback, which bases on the large difference between the albedo values of water and sea ice. Proxy data shows evidence for at least 4-5°C increased summer temperatures in most of the arctic regions (CAPE-Last Interglacial Project Members, 2006; Axford et al., 2011). Fossils in northeast Siberia indicate, that the tree line was shifted northward at least 270 km northward (Kienast et al., 2011). NEEM Greenland ice core data state air temperatures that were even 8°C higher during the Eemian interglacial compared to the last millennial average in Greenland (NEEM Community Members, 2013). There are suggestions, which explain these high temperatures and climate changes not only by polar amplification but also with intensified North Atlantic drift, leading warm water into the Arctic Ocean (CAPE-Last Interglacial Project Members, 2006). On the other hand, there are studies with evidence for relative cold Eemian SSTs from the Nordic Seas (Bauch et al., 2012). A warmer Arctic Ocean would probably lead to increased precipitation over coastal Siberia, which is contraindicated by evidence for dry continental climate (Kienast et al., 2011). The coexistence of high northern land temperatures and a still large Greenland ice sheet, as well as rather low sea temperatures, seem to stand in contradiction to each other. This highly emphasizes the need for further proxy data, which is yet missing from the Bering Sea.

3. Methods

3.1. Used samples and datasets

All samples were taken from core SO 201-2-85KL. This core was recovered using piston coring from the Shirshov Ridge (57°30.3080'N, 170°24.7700'E). Water depth at core location is 968 m, total core recovery 1813 cm (Dullo et al., 2009). This area is applicable, because it has a high sedimentation rate, which is necessary for a sufficient resolution. Another advantage of the location is that it is not too far to the north and not too close to the shore, so that it is ice-free throughout the year in the modern situation (**Fig.4, p.9**). Proxy evidence in this core for IP_{25} during glacial termination I (Max et al., 2012) allows assuming that there was at least seasonal sea ice during MIS 6 and glacial termination II. Therefore a change between occurrence and absence of sea ice between both stadiums can be expected, which helps interpreting the process of glacial/interglacial transition. Additionally the area of the Shirshov Ridge is affected by the western Bering Sea current, which leads water masses to the North-Pacific via

the Kamchatka strait and may be involved by the formation of NPIW during glacials, which emphases the oceanographic importance of this location **(Fig.1, p.6)**. To compare the samples with other data a variety of datasets were used. This includes mainly SST reconstructions from locations in the Bering Sea, North Pacific and North Atlantic. Additional the age model, Total organic carbon (TOC) and color b* values were taken from external data for core SO 201-2-85KL. All used datasets are stated in **Table 1**.

Core	Used Parameters	Region	Reference
SO 201-2-85KL	Age model, TOC, color b*; Holocene SST ($U^{K'}_{37}$)	Shirshov Ridge (W Bering Sea)	Riethdorf et al. (2012); Max et al. (2012)
SO 201-2-77KL	SST ($U^{K'}_{37}$)	Shirshov Ridge (W Bering Sea)	Max et al. (2012)
SO 201-2-101KL	SST ($U^{K'}_{37}$)	Shirshov Ridge (W Bering Sea)	Max et al. (2012)
M23414	SST (planktic foraminifera); age model	Rockall Plateau (E North Atlantic)	Bauch et al. (2012)
MD01-2444	SST ($U^{K'}_{37}$)	Iberian margin	Martrat et al. (2007)
ODP 108-658	SST ($U^{K'}_{37}$)	W of Cape Blanc (W African coast)	Eglinton (1992)
ODP 145-882	SST ($U^{K'}_{37}$)	NW North Pacific	Martinez-Garcia et al. (2010)
ODP 167-1018	SST ($U^{K'}_{37}$)	Californian margin	Mangelsdorf et al. 2000)
MD 97-2151	SST ($U^{K'}_{37}$)	South China Sea	Zhao et al. (2006)

Table 1: used datasets

3.2. Extraction

For this thesis, 79 samples were analysed. The samples cover the time range over MIS 5 and focuses on MIS 5e. The sample depth were chosen according to the age model, taking into account global isotope records in order to have a better resolution during periods of climate change.
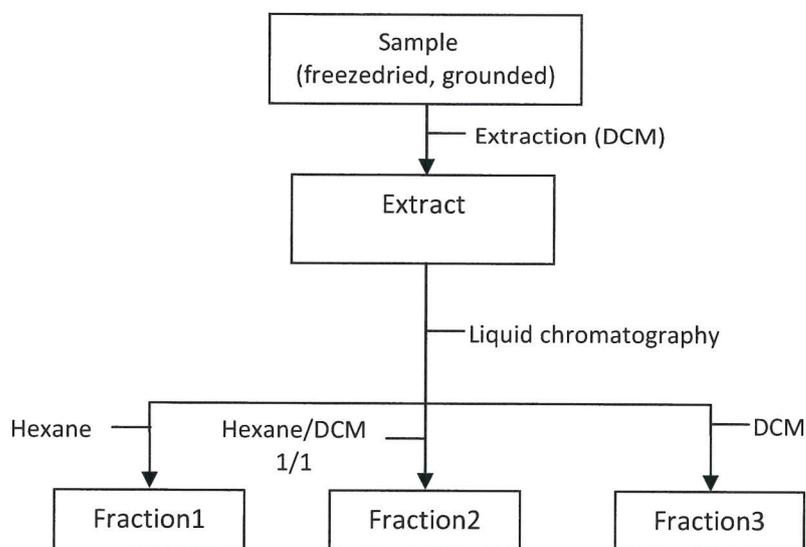
Figure 6: Schematic of extraction procedure

Samples were freeze-dried and grounded. C:26 was used as internal standard. Lipids were extracted using an accelerated solvent extractor (ASE) from Dionex type 350. Extraction was done using dichloromethane (DCM) as solvent. Two samples were extracted in advance to adjust the method to the requirements of the samples. Both test samples were cleaned from organic compounds with high polarity like alcohols and fatty acids by liquid chromatography. Columns were conditioned with three columns hexane. Samples were transferred on columns using hexane. Chromatography was done with 4 ml DCM. Columned samples were vaporised via rotary evaporator with 120 rpm at 43°C. Pressure was 500 mbar and was reduced after evaporation of DCM to 325 mbar. Complete evaporation of solvents was achieved with nitrogen gas. After this samples were solved in hexane.

Both test samples showed distracting GC signals at the same retention time as alkenones from an external standard. All samples including new samples from the same depth as test samples were extracted as shown in **Figure 6**. Extracted lipids were vaporized and dissolved in hexane, then separated in three fractions using liquid chromatography with silica gel columns. Silica columns had a length of 5 cm. Columns were conditioned with two ml DCM and five ml hexane. Separation was done by elution with hexane (5 ml as F1), hexane-DCM (1:1, 5 ml

as F2) and DCM (5 ml as F3). By this separation, the alkenones are dissolved in F3, and IP_{25} is included in F1. All fractions were vaporised via rotary evaporator with 120 rpm at 43°C. Pressure was 325 mbar (F1), 500 mbar and after evaporation of DCM was reduced to 325 mbar (F2) and 730 mbar (F3). Complete evaporation of solvents was achieved with nitrogen gas. After this samples were solved in hexane.

Fraction 3 was analysed using a gas chromatograph (Agilent 7890A with cold injection system) with flame ionisation detector (GC-FID). Before measuring all samples were vaporized and dissolved in hexane. Alkenone peaks were identified, by overlays with chromatograms of an external standard, with an alkenone temperature of 10°C. GC was equipped with a DB1MS fused silica capillary column (60 m x 0,25 mm inner diameter (i.d.), 0.25 µm film). The samples were injected at 60°C. After three minutes temperature was raised by 20°C per minute up to 150°C, then up to 320°C at a rate of 6°C per minute and finally kept at 320°C for 40 minutes. Carrier gas was helium at a flow rate of 1:5 ml/min. Alkenones were not measured quantitatively, because the finally used method separated the available internal standard (C26, F1), from the alkenones. It would have been possible to mix again F1 and F3 in order to measure the concentration, but only by taking a high risk of inaccuracy.

For IP_{25} analyses F1 was analysed with a gas chromatograph coupled with a mass spectrometer (GC-MS). GC was type Agilent 6850 (HP-5MS column, 30 m x 0.25 mm i.d., 0.25 µm film), coupled to an Agilent 5975 C VL mass selective detector. Temperature program started at 60°C, held for three minutes. Then, temperature was raised by 15°C/min up to 150°C, then up to 320°C at a rate of 10°C/min and kept at 320°C for 15 minutes. Carrier gas was helium. Mass spectrometer was operated with an ion source temperature of 230°C and ionisation energy of 70 eV. IP25 was identified by comparison of retention time and mass spectra to published data (Belt et al., 2007).

In some cases the concentration of alkenones were insufficient, to integrate peaks, so that it was necessary to measure samples again with less hexane, in order to increase peak intensity. In most of the repeated measurements the alkenone concentration was too low, so that the second measurement could not improve the signal. Three samples were controlled in F2 and showed signals analogue to alkenones, according to external standard, but with several disturbing signals surrounding them. All three samples were separated again with liquid chromatography as described above and then measured in F3, but still showed no reliable signal.

3.3. Used Proxies

Sea surface temperature ($U^{K'}_{37}$)

Today there are several proxies, which allow reconstructions of sea surface temperatures from marine sediments. This includes Mg/Ca ratios and stable isotopes from planktic Foraminifera as well as biomarker like $U^{K'}_{37}$. During glacial termination the top layer of low salinity water leads to a stratification of the water column (Katsuki & Takahashi 2005). Therefore SST reconstructions via planktic Foraminifera, (for example Barker et al., 2005), may lead to misinterpretation of the SST-signal, as it cannot be excluded, that the calculated temperatures reflect the conditions below the thermocline. Furthermore recent published SST data from the Bering Sea is based on alkenones and there are still problems comparing SSTs which are reconstructed via different methods (Leduc et al., 2010). Due to this reasons, the Eemian SST was reconstructed using the $U^{K'}_{37}$ proxy.

The reconstruction of the sea surface temperature is done via the U^{K}_{37} index. This index is the ratio between three different species of alkenone C37, which differ from each other by their number of double bonds (Brassel et al., 1986). The ratio between the species is temperature depended. But there are also other factors influencing the ratio, which should be considered, like low abundance of nutrience, or insufficient light (Prahl et al., 2006). The species C37:4 mainly occurs at very cold temperatures (Prahl et al., 1988) and is preferred target of decomposition (Sikes et al. 1997). Therefore, for comparison at global scale, normally the $U^{K'}_{37}$ index is used, which ignores C37:4, as stated in **Equation.1** (e.g. Müller et al., 1998).

$$U^{K'}_{37} = \frac{[37:2]}{[37:2]+[37:3]}$$

Equation 1(Müller et al., 1998)

To calculate the SST via the $U^{K'}_{37}$ index a calibration is used. There are calibrations varying on temperature ranges or certain latitudes. In order to get the most accurate temperature, it would be ideal to use a local calibration for the Bering Sea, derived from sediment tops. Such a calibration is not available yet. Important calibrations are Prahl et al. (1988), based on laboratory measurements, Müller et al. (1998), based on global sediment tops (until ±60° latitude), and Sikes et al. (1997) which focuses on sediment samples from the Southern Ocean, and represents late summer temperatures. In low and middle latitudes the calibrations after

Prahl et al. (1988) and Müller et al. (1998) represent annual mean temperatures. This depends on the seasonality of alkenone production. In the modern Bering Sea the main bloom of *Emiliania huxleyi* is during September which implies that calculated SST are likely to reflect late summer temperatures (Harada et al., 2003).

In **Figure 7** these three calibrations are used to calculate possible SST values. The calibrations after Prahl et al. (1988) and Müller et al. (1998) are practically identical. SSTs calculated after Sikes et al. (1997) show similar behavior of the curve, but with general increased temperatures of more than 2°C. Modern average September SST compared to surface sediment samples, showed the best correlation to Sikes et al. (1997) calibration (Harada et al., 2003).
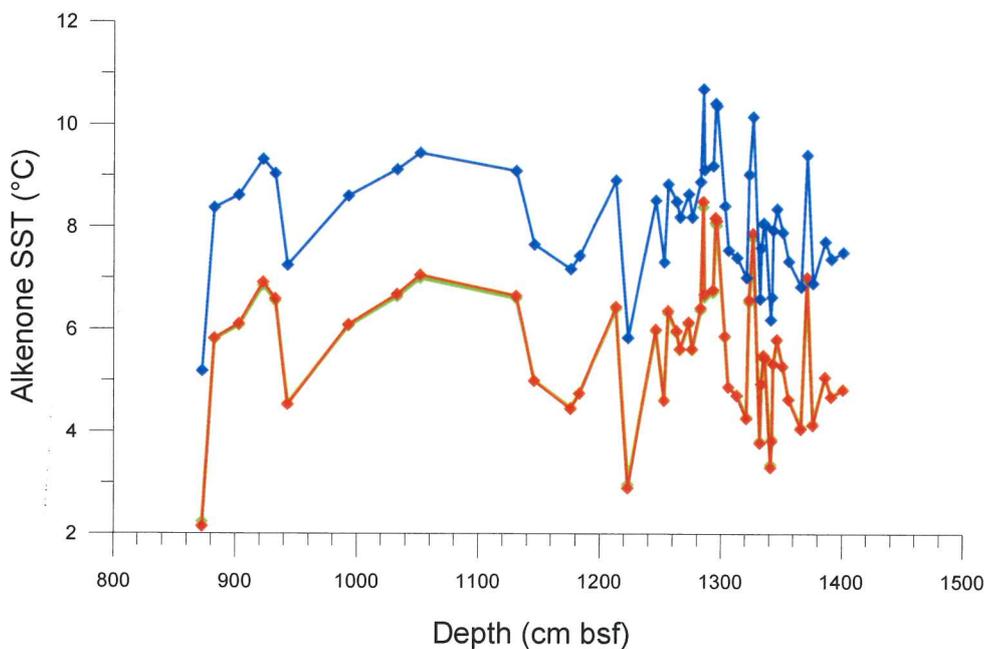
Figure 7: Calculated SST after different calibrations

SST calculated with $U^{K'}_{37}$ calibration after Sikes et al. (1997) (blue line); Müller et al. (1998), (green line); and Prahl et al.(1988) (red line).

Recent published paleo-temperatures from the Holocene in the Bering Sea were all calculated using the calibration after Müller et al., (1998) . Additional the most published alkenone derived SST data from the Atlantic and Pacific using either the calibration after Müller et al. (1998) or Prahl et al. (1988). As one of the main scientific aims of this thesis is to compare the reconstructed SSTs to these values, the Müller et al. (1998) calibration was chosen (**Eq.2**).

$$U_{37}^{K'} = 0.033T\ [°C] + 0.044$$

Equation 2 (Müller et al., 1998)

Solved towards T, the calculation results in **Equation 3**

$$T\ [°C] = \frac{U_{37}^{K'} - 0.044}{0.033}$$

Equation 3

Sea ice occurrence IP_{25}

To reconstruct the occurrence of sea ice, the IP_{25} proxy is used. IP_{25} is a monounsaturated C_{25} highly branched hydrocarbon (**Fig.8**). It is produced by diatoms living within the lower side of annual sea ice, which makes it a proxy for at least seasonal sea ice. IP_{25} producing diatoms are depending on light, so they are not to be found during periods of thick perennial sea ice covers (Belt et al. 2007). To get more distinctive results Müller et al. (2011) proposed to add the concentration of brassicasterol, a biomarker for marine phytoplankton, to the proxy. This allows a more detailed reconstruction regarding the sea ice cover, because it solves the problem which occurs with an absence of IP_{25}, which can indicate an ice free water surface as well as thick multi annual ice cover. However in this thesis, only the qualitative analysis was taken. This was done, because the main focus was laid on SST reconstruction. Brassicasterol as part of the alcohol fraction would have made the extraction and chromatography process more complex and time consuming, leading to less SST results. The above mentioned problem of the ambiguity of IP_{25} absence can be avoided otherwise. The presence of alkenones is an indicator for at least seasonal ice free surface water (Armand & Leventer, 2010).
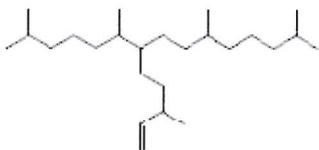
Figure 8: Chemical structure of IP_{25} (Belt et al., 2007)

3.4. Age model

Though for the core SO 201-2-85KL, an age model already existed, it was still a matter of discussion during the creation of this thesis especially regarding glacial termination II. In this thesis the newest available age model after Riethdorf et al. (2012) was used. The part for MIS

5 before 122 ka BP is based on correlation of color b* values to the $\delta^{18}O$ record of NGRIP ice core. Below that color b* and Ca/Ti log ratios (XRF scanning) were correlated to the Sanbao stalagmite $\delta^{18}O$ record (Riethdorf et al., 2012). The given age model was adjusted to each sample depth by linear interpolation of the closest surrounding points (**Fig.9**).
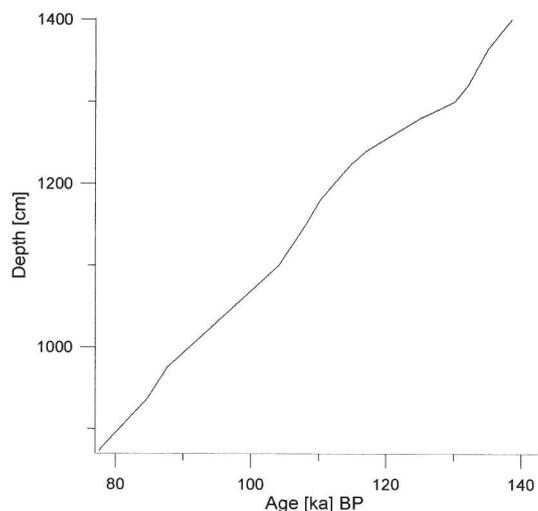
Figure 9: Depth to age correlation of core SO 201-2-85 KL

Data source: Riethdorf et al., (2012).

3.5. Linear sedimentation rate

The linear sedimentation rate (LSR) depends amongst other factors on terrigenous sediment input and biogenic production (Fütterer, 2006). Combined with other proxies (e.g. TOC and carbonate) it allows reconstruction of the magnitude of both factors. It was calculated for each cm from the age model according to **Equation 4**

$$LSR = \frac{\Delta depth\ [cm]}{\Delta age\ [ka]}$$

Equation 4

4. Results

4.1. SST reconstruction

In 56 out of 79 analyzed samples from this study, alkenones could be detected and SSTs were calculated. In 23 Samples either alkenones were not detectable or the concentration was too low to calculate a reliable $U^{K'}_{37}$-index.

The calculated sea surface temperatures are plotted in **Figure 10**. In general the SST curve correlates with global trends, indicated by the Greenland Ice core record NGRIP (Rasmussen et al., 2006) and the marine isotope stack by Lisiecky and Raymo (2004) (LR04). So the marine isotope sub-stages 5a to 5e can be identified clearly. Before glacial termination II at 135 ka BP the temperature oscillates around 5°C with a peak up to 7°C at 140 ka BP and is followed by a drop to temperatures below 3.5°C. During the transition between MIS 6/5e and in early MIS 5e, there is a saw tooth shaped increase up to 8°C at 128 ka BP. The latter half of MIS 5e is dominated by a steep decreasing trend towards MIS 5d, interrupted by an outlying high temperature of 8.5°C at 124 ka BP, directly surrounded with samples, which have temperatures well below 7°C.

The decline at the transition between MIS 5e and d, which results in a temperature minimum of 3° at 115 ka BP, is accompanied with an absence of alkenones. Therefore it was not possible to reassure this trend with supporting data-points. Towards the slightly warmer stage 5c the temperature curve again follows a saw tooth shaped increase. It is supported by few data only, because nine samples within this time period do not contain sufficient concentrations of alkenones. Therefore, the cold phase at the beginning of MIS 5c around 105 ka BP, which is observed in the NGRIP isotope curve and the color b* dataset from core SO201-2-85KL, is not represented in the SST data. In MIS 5c the temperature climaxes with 7.1°C at 97 ka BP.

After this, during sub-stage 5b, the temperature curve describes a long moderate drop down to 4.5°C at 85 ka BP. A short warm phase during this period, indicated by NGRIP and color b* data, is not observed in the temperature record, but can also not be excluded due to low resolution. The warm sub-stage MIS 5a is rather short and correlates well to the LR04 Stack, the NGRIP isotope curve and the color b* data. MIS 5a culminates around 83 ka BP at a temperature of about 7°C, which corresponds to the maximum during 5c.
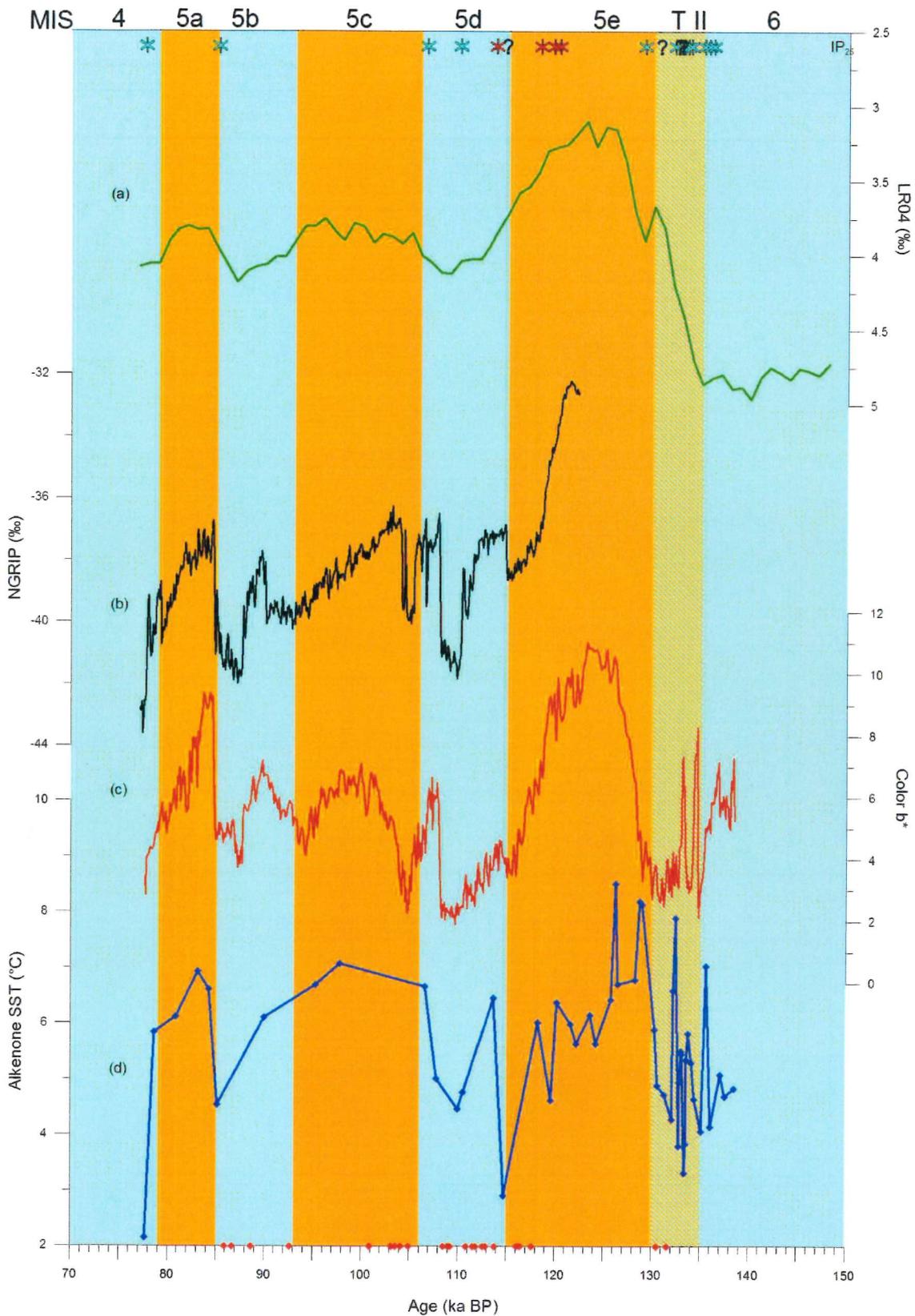
Figure 10: MIS 5 SST, reconstructed with U$^{K'}_{37}$.

Red diamonds at the bottom represent samples with insufficient alkenone content (d); spectro-photometric measurements (c) (color b*, Riethdorf et al. (2012)), from core SO 201-2-85 KL plotted against the NGRIP isotope record (b) (Rasmussen et al., 2006) and the benthic isotope stack LR04 (a) (Lisiecki & Raymo, 2005). Blue stars indicate presence, red stars absence of IP$_{25}$ in core SO 201-2-85 KL. Question marks represent samples with IP$_{25}$ Concentration close to detection limits. Warm periods are marked orange cold periods ice blue.

Towards MIS 4 the SST decreases strongly towards the lowest calculated value in this thesis, 2.2°C at 77 ka BP. The samples which contained too low alkenone concentrations to calculate accurate SSTs concentrate on MIS 5d and early 5c and in smaller amount during MIS 6/5e transition and in MIS 5b.

4.2. Reconstruction of sea ice occurrence

IP_{25} could be found in 12 samples, whereas four samples contained only quantities near detection limits and 4 samples were free of IP_{25}. All samples during MIS 6 and in the beginning of glacial termination II contained IP_{25} (**Figure 10**). At the ages of 130 and 132.5 ka BP the IP_{25} concentration was near detection limits, but in between at 132 ka BP IP_{25} could be detected. During MIS 5e, only at 128 ka BP, parallel to the first SST peak during this sub-stage, IP_{25} can be observed. During the short cold phase in early MIS 5d IP_{25} was only found near detection limit, followed by a complete absence at 113 ka BP. In late MIS 5d IP_{25} is present also during the temperature increase at the 5d/5c transition. IP_{25} was also detected at the temperature minima before and after MIS 5a.

4.3. Error analysis

Improper lab procedures during column chromatography could have disturbed the segregation process, so that alkenones might end up in fraction II. In three samples, with very low alkenone concentration, fraction II was checked and showed alkenone like signals, with strong disturbances. All three samples went again through column chromatography but did not show any improvement. The GC analysis was done in 7 sessions. In each session an external standard was measured as first and last sample, with a standard alkenone temperature of 10°C, which was not only used to identify alkenones, but also to check technical drift. Additional errors can be generated during manual signal integration, which is depending on signal intensity. Samples with very low intensities were therefore measured again with less hexane, in order to increase alkenone concentration, and so to manage this error source. In most cases the intensified signal, could not be integrated though, because disturbing signals were also intensified or made identification of alkenones impossible. Samples where this method worked are marked in the annex (**Table 2**). Checking the external standard temperature, analytical errors could be determined between ± 0.2 and 0.6°C which lies within the standard deviation for the Calibration after Müller et al. (1998) of ± 1°C.

5. Discussion

5.1. Possible reasons for low alkenone abundance

To put the results into context and to be able to assess causes of low alkenone concentration, total organic carbon (TOC), the linear sedimentation rate (LSR) and Color b* are taken into account. Color b* is a photometric value, which can be used to identify variations in diatom-derived opal content and in terrigenous organic matter (Debret et al., 2006). The total organic carbon content (TOC), combined with the sedimentation rate, helps to make assumptions about the source of organic matter (Rullkötter, 2005).
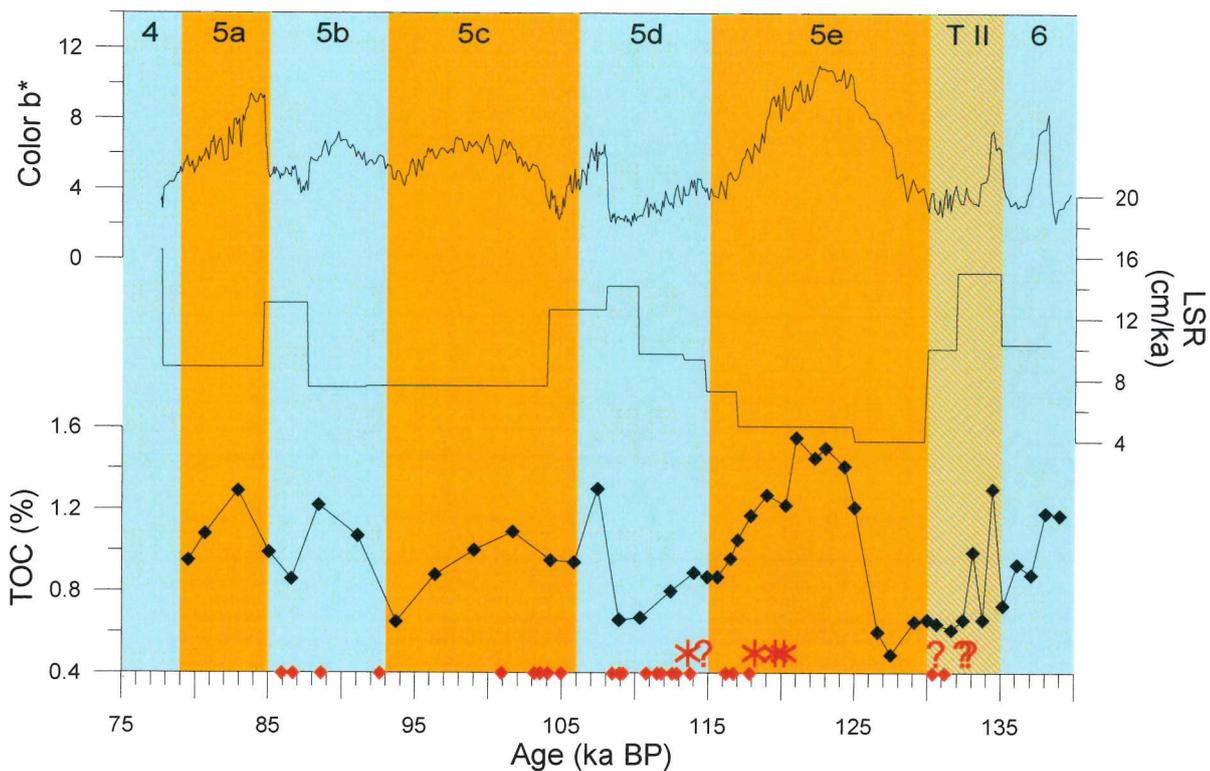
Figure 11: Additional data from core SO201-2-85KL sediments.

Color b*, total organic carbon and linear sedimentation rate against age. Red diamonds indicate samples with no or very low alkenone concentrations. Numbers on top indicate marine isotope stages. Red stars and question marks display samples with no or very low IP$_{25}$. Content Light blue background color indicates cold phases, orange warm phases. Data source: Riethdorf et al. (2012)

These sediment parameters are plotted over time in **Figure 11**. Color b* and TOC values show a good correlation throughout MIS 5. Both parameters generally show high values during warm periods and low values during cold periods, and run mostly parallel to the SST curve. The sedimentation rate is anti-correlated to these patterns, except for the begin of TII,

the beginning of the MIS 5e and 5d/5c transition, where the behavior is similar to the other proxies.

Samples with no or very low alkenone concentrations mostly correlate with low TOC values, especially during glacial termination II, during the beginnings of MIS 5d and 5c and the end of 5b. In the first two cases this applies also for IP_{25}. This correlation indicates that the absence of alkenones and IP_{25} is probably neither caused by a specifically low abundance of *Emiliana huxleyi* or IP_{25} producing diatoms, nor a specific degradation of alkenones or IP_{25}, but by factors affecting all kinds of organic structures. This can include biologic reasons like low production in general. Another cause can be factors that affect the composition of the sediment.

High terrestrial input with low organic carbon content can lead to elusion of organic matter (Rullkötter, 2005). This is also visible in **Figure 11** and the correlation of high LSRs, small color b* values and low TOC content. Terrigenous material in core SO201-2-85KL is found mainly during cold periods and in the beginning of deglaciation phases (TII, MIS 5d and 5b). The suggested main source is sea ice rafted debris from the north (Riethdorf et al. 2012). During warm periods like MIS 5e, the proxies show an opposite behavior indicating low terrigenous and high marine sediment input.

Another important factor concerning the TOC concentration of sediments is organic decay. Decay rates of organic material are strongly controlled by the oxygen content of the uppermost part of the sediment and therefore influenced by the oxygen content of the bottom water (Hensen et al., 2005). Phases with low TOC contents, parallel to a low sedimentation rate to exclude elusion, are a possible indicator for improved bottom water ventilation, which can be caused by deep or at least intermediate water formation. The most prominent examples of this condition in core SO201-2-85KL are observed during glacial termination II and in early MIS 5d (115-110 ka BP) which is also a period with very low alkenone concentration. This correlates well with a suggested onset of NPIW formation during early MIS 5d in western Bering Sea (Horikawa et al., 2010).

There are two samples at 89 and 101 ka BP and three samples between 116 and 118 ka BP, where very low alkenone abundance coincides with high TOC. This might be explained by factors which affect the production of haptophytes or specific degradation of alkenones. Possible errors in lab results could also provide an explanation for this discrepancy.

5.2. Origin of measured alkenones

One factor which can lead to misinterpretation of biomarkers can be allochthonous organic matter. In this study, that would be the case if alkenones found in the samples, were originally produced in a distant area or deposited in other layers. Then, the reconstructed temperature would not reflect the environmental condition at the core location in the age determined by the age model. The two main sources for allochthone sediment are terrigenous input and the redeposition of eroded sediment (Rullkötter, 2005). Apart from processes which affect the sediment, the transport of organic matter through the water column might play the major role in a dislocated temperature signal.

As already stated, terrigenous material probably originates from sea ice rafted debris from the north and is most abundant at the end of glacial periods. These phases go along with low TOC contents (see **Fig.11, p.22**). Riethdorf et al. (2012) recently published C/N ratios in MIS5, which mostly varied between 10 and 11. One maximum was reached during the beginning of the last interglacial (ca. 125 ka BP), with smoothed C/N values up to 15. Ratios of 10 are typically a sign for marine-derived matter, while average terrigenous organic matter has C/N ratios of 20 or higher (Rullkötter 2005). This means that over the most part of MIS 5, the organic matter is primarily of marine sources and the most possible time slice for possible confusing terrigenous organic matter is around 125 ka BP.

The other possible source for dislocated organic matter could be redeposition. Turbidity currents can be excluded, because neither were there turbidites in the core, nor were there discontinuities in the age model. However, at the beginning of glacial termination II (ca. 134 ka BP) there is a high sedimentation rate which goes along with high TOC and color b* values **(Fig.11, p.22)**. Therefore, alien marine organic matter cannot be completely excluded at this age without stable isotope measurements.

A shift of organic matter via horizontal transport through the water column might be the highest uncertainty. As already mentioned, the main direction of water currents at the core location is northward. The velocity of bottom currents can be regarded as low, due to repeated occurrence of laminated sediments (Dullo et al., 2009). The Holocene SST curves of cores SO201-2-77KL, SO201-2-85KL and SO201-2-101KL as plotted in **Figure 12(p. 26)**, show a south to north transect. The SST curves have almost the same patterns, but differ regarding absolute temperature, with lower temperatures in northern locations. Taking all these arguments into account, the possibility of shifted material cannot be excluded, but rather regarded as low.

5.3. Comparison of Eemian and Holocene surface temperature

As mentioned in the introduction, Holocene and Eemian insolation follow the same temporal patterns, but with different intensities **(Fig.5, p.10)**. To compare Eemian and Holocene SST, it is important to choose an applicable synchronization of both timescales. In order to avoid stretching or compression of the datasets, time strips with the same length were chosen. To achieve the best possible comparison regarding the state of the climate, both time scales are arranged, as visible in **Figure 12a**, according to the best congruence of the summer insolation curve. Holocene SST records were taken from core SO201-2-85KL as well as from cores SO201-2-77KL and SO201-2-101KL (core details **Tab.1**) (Max et al., 2012). These three cores are part of a North-South transect on the Shirshov Ridge. The Holocene record is limited because of low alkenone abundance before 14 ka BP. for better comparison, only the comparable part of the MIS 5 record was plotted.

Both records from core 85 show values within the same variability range, between 3 and 9°C. Parallel to Bølling/Allerød, a warm phase at the end of the last glacial, a warming trend is visible. However, the first Eemian temperature peak corresponds to the minima of the Younger Dryas (YD), which looks like anti-correlated behavior. The time lines were shifted **(Fig.12b)** in order to archieve the best possible correlation of both SST curves without stretching or compressing the time lines. The new Eemian section lies 2 ka earlier, the new Holocene sectrion one ka later, resulting in an insolation curve phase shift of 3 ka.

Comparing the SST curves according to this arrangement, the trends are similar. The Eemian curve has corresponding temperature maxima to the Bölling/Allerød (B/A) and the Holocene thermal maximum and there is a large temperature drop, which correlates to the Younger Dryas (YD). However, the congruence of both curves is still a bit displaced, so that an actual phase shift of 2.5-3 ka can be assumed.

One possible explanation for this shift is stratigraphic inaccuracy. This inaccuracy is probably concentrated on the Eemian dataset, because the Holocene age model of all three cores is well backed up by absolute C^{14} ages (Max et al., 2012). The length of warm and cold phases during glacial termination II and the early Eemian generally fits with the length of corresponding phases during the Holocene. Therefore, the error seems to originate mainly in absolute age, not in the time relation of the curve itself. There is another possible factor which might be responsible for the phase shift, additionally to a stratigraphic inaccuracy. Insolation is thought to be one of the main climate drivers of both interglacials within the Bering Sea (Riethdorf et al., 2012). After 136 ka BP. the Eemian summer insolation has a steeper increase than the
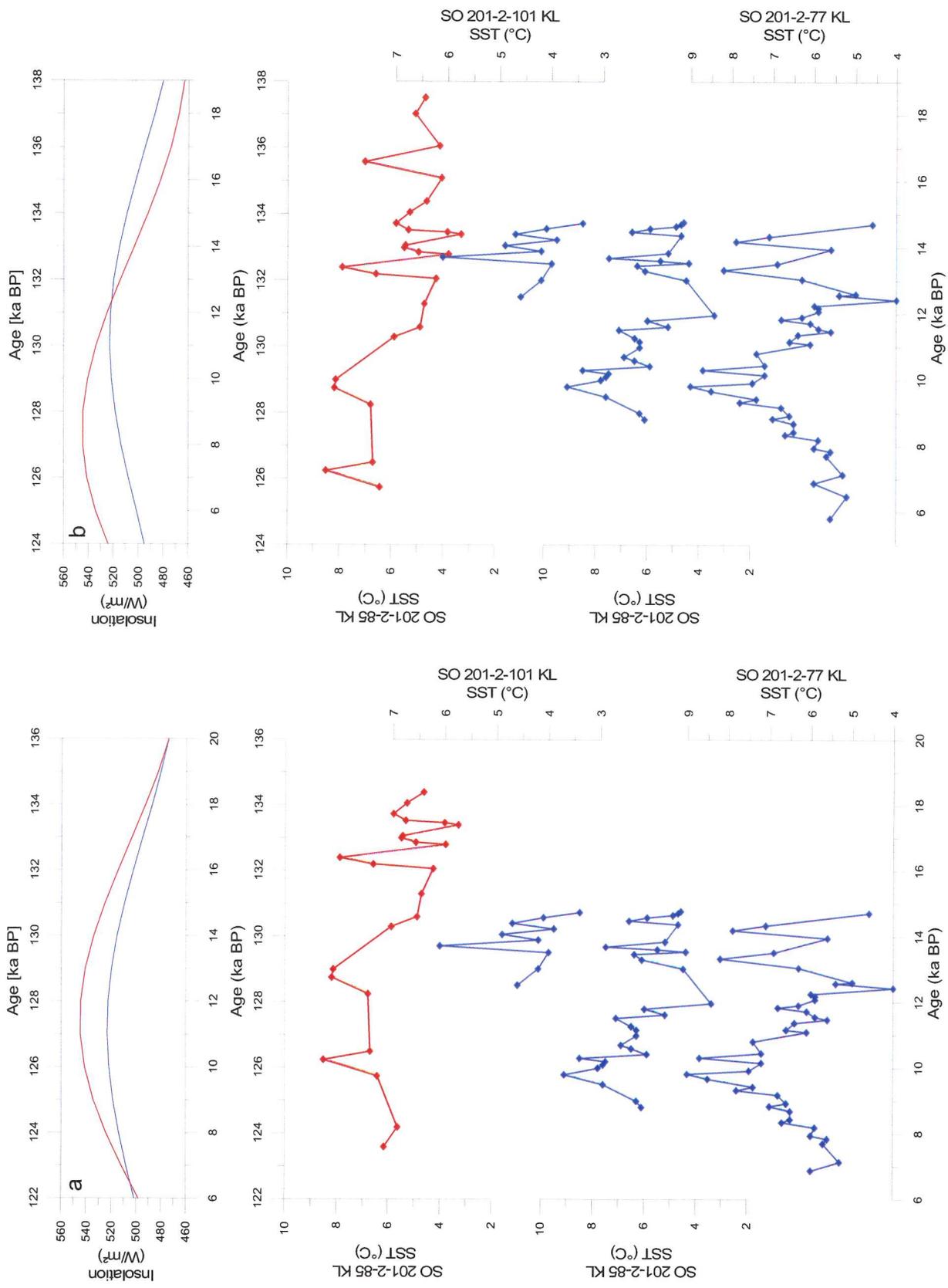
Figure 12: Eemian and Holocene SST. Curves on top are Eemian and Holocene June insolation curves (65°N) (Berger & Loutre, 1991). Timelines of temperature records are compared via greatest correlation of insolation (a), and greatest correlation of SST (b). Red lines indicate Eemian, blue lines Holocene records (Max et al., 2012).

Holocene at the same stage (**Fig.12**). This might result in an accelerated deglaciation process.

Apart from the cause of the shift in insolation-temperature relation, the SST curves show a very similar behavior. The glacial termination begins with a short but intense temperature increase, followed by a rapid temperature drop back to the glacial level for a period of less than 2 ka, resulting in a prolonged warming trend. In the Eemian pattern, this second warm phase does not reach much higher temperatures than the first one, while the Holocene shows peak temperatures during the Holocene thermal maximum (HTM) that are more than 1°C higher than during the first warm phase, the Bølling/Allerød (B/A).

Surprisingly, the higher Eemian peak insolation did not lead to higher SST in the Bering Sea. This is more surprising considering the assumed global mean temperature increase of 2°C. Recent studies like Axford et al. (2011) and NEEM (2013) presented proxy data with Eemian peak air temperatures in the arctic that were 8°C higher than the preindustrial values. These high temperatures are explained not only by the higher insolation, but by the resulting induced polar amplification like ice-albedo feedback and an increased meridional heat transfer from the sub-polar North Atlantic into the Arctic sea (CAPE, 2006). (Bauch et al., 2012)

5.4. MIS 5 temperature development in the North Pacific

As stated in the introduction, the Bering Sea is not only affected by the Pacific Ocean via currents, but mainly via atmospheric teleconnections that control the strength and position of the Aleutian low. **Figure 13** compares SST curves from the North Pacific with the Bering Sea record. For the purpose of comparison, three SST records that cover the North Pacific were chosen. The most northern data set is from core ODP 145-882 located off Kamchatka Peninsula (Martinez-Garcia et al., 2010). Despite its rather poor resolution it was chosen, because the core location is influenced by the Kamchatka current. The mid-latitude core ODP 176-1018, lies west of California (Mangelsdorf et al., 2000) and MD97-2151 lies in sub-tropic South Chinese Sea east of Vietnam (Zhao et al., 2001). All three records are derived from alkenones, using the Prahl et al. (1988) calibration and do not represent summer, but annual mean temperatures. Core details are stated in **Table.1**. In the two northern N-Pacific cores the resolution during Termination II is too low for comparison. The core MD97-2151 shows far less variability than core SO 201-2-85KL, with a temperature range within 1°C. This stable phase begins and ends with a temperature rise. A high temperature dynamic, such as the SST rise and a subsequent drop at 131 ka BP which is very prominent in core SO 201-2-85KL,
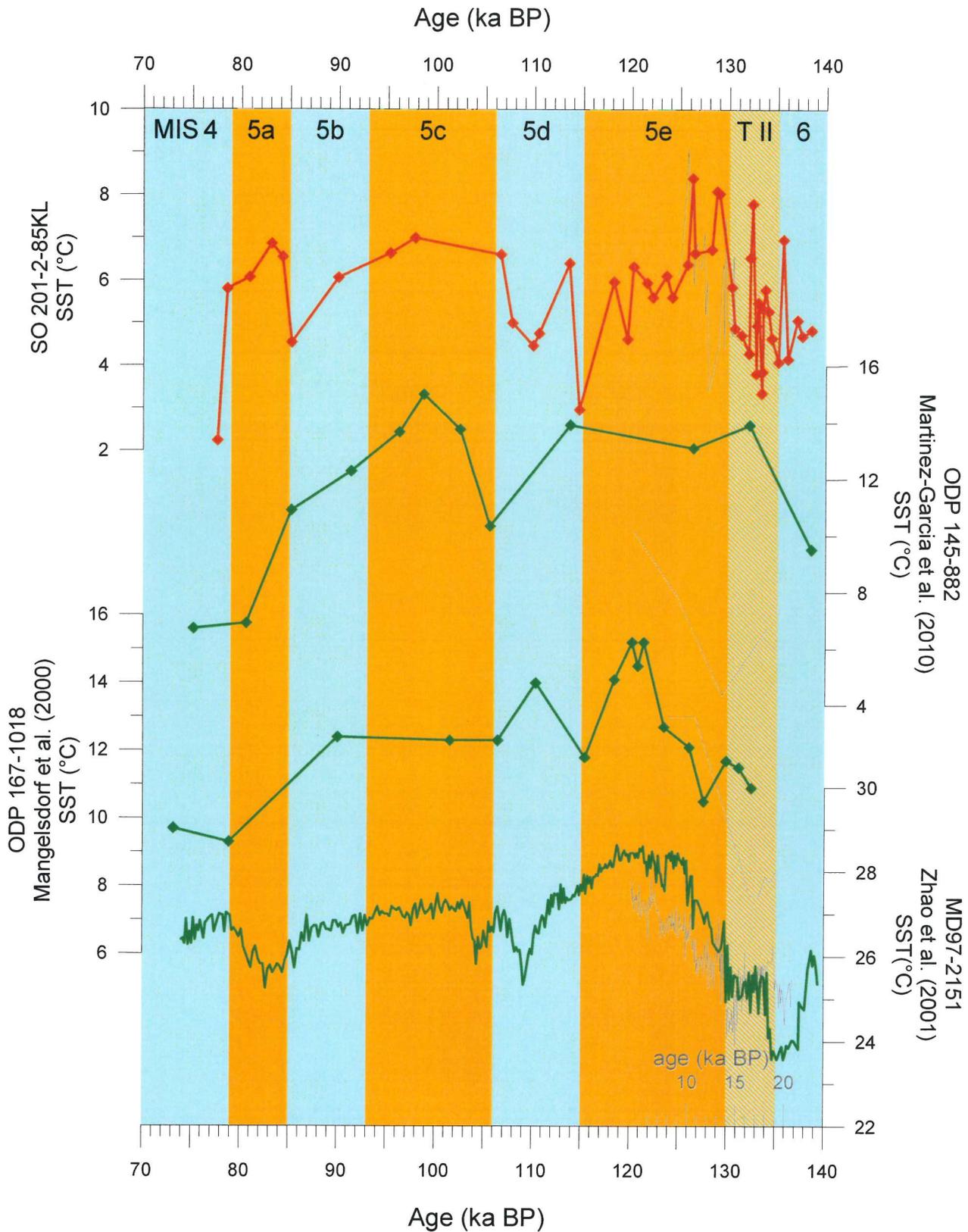
Figure 13: MIS 5 SST from the Bering Sea and the North Pacific.

The red graph indicates Bering Sea temperature curves, whereas green lines show Pacific temperature curves. Grey lines show Holocene SST records to each core, which are related to the grey axis at the bottom (SO201-2-85KL: Max et al. (2012)). For core details see **Table 1.** Numbers on top indicate marine isotope stages. Light blue background color indicates cold phases, orange warm phases.

cannot be found. The Eemian is represented in the Bering Sea SST record by a steep increase followed by a moderate descending trend. Except core ODP 145-882, this pattern is reversed by the Pacific temperature curves. After MIS 5e, the northern and the southern Pacific temperature records follow generally the same temperature patterns as core SO 201-2-85KL. During the transition between MIS 5c and 5b where the data point density of core ODP 145-882 is comparable to the Bering Sea record, both curves show a very parallel trend. Except the mid latitude core ODP 176-1018, where MIS 5d and 5c reflect reversed trends. No evidence of increased SST during MIS 5a can be seen in any of the plotted Pacific SST curves.

Figure 13 also contains the Holocene SST records of each core. Time lines are synchronized as in **Figure 12a (p. 26)**. As during MIS 5e resolution of ODP 145-882 during glacial termination I and the early Holocene allows only a superficial analyses. Clearly visible is the YD which seems to be parallel to SO 201-2-85KL. The Holocene temperatures stay well below the Eemian level. The maximum Holocene SSTs from core ODP 167-1018 are ca. 2°C higher than the Peak in MIS 5e. According to the chosen comparison of time lines, Glacial termination II is delayed towards termination I.

SST development of core MD97-2151 during termination I is parallel to termination II, with the difference that in termination I there is a cool event (YD) before the warming trend. In general the correlation of this core compared to the Bering Sea SST curve is better during the Holocene than during the Eemian interglacial. MIS 5e shows an enhanced temperature of 1-2°C compared to the Holocene.

5.5. MIS 5 temperature development in the North Atlantic

During interglacials, the North Atlantic Ocean is indirectly connected, via the Arctic Ocean, to the Bering Sea. A more important role, is suspected to lay in atmospheric teleconnections. As mentioned before, climate models suggest a temperature seesaw between the North Atlantic and North Pacific during the late Holocene (Kim et al., 2004) while recent Holocene SST records from the Bering Sea and the sub-arctic N-Pacific found evidence of parallel temperature development in both realms. **Figure 14** compares SST curves from the North Atlantic with the Bering Sea record. For the purpose of comparison three SST records that cover the North Atlantic were chosen. The most Northern data set is from core M23414, which originates from Rockall Bank, NW of Ireland (Bauch et al., 2012). The mid latitude-core MD01-2444 lies off the Spanish west coast Martrat et al. (2007), and core ODP108-658 lies west of
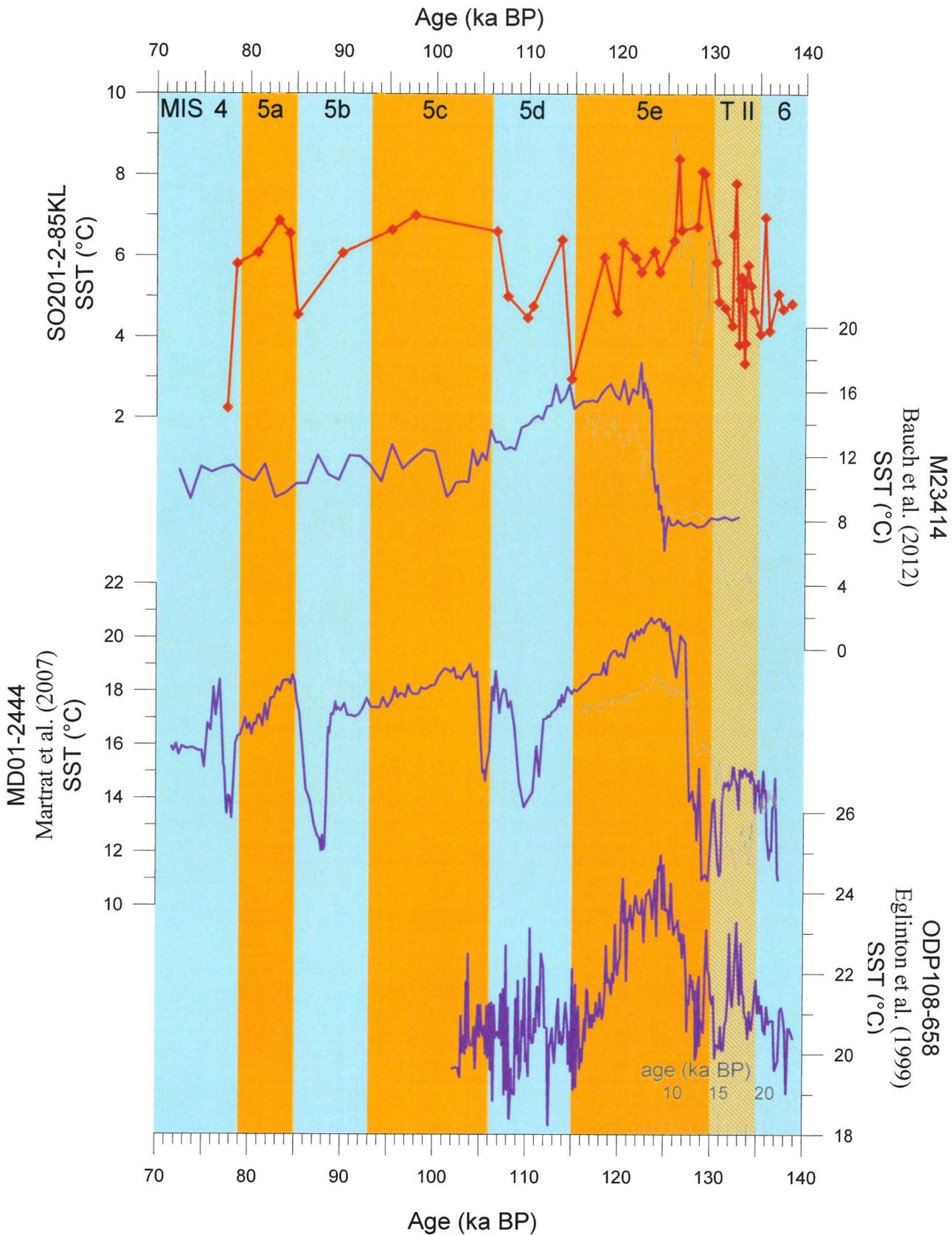
Figure 14: MIS 5 SST from the Bering Sea and the North Atlantic.

The red graph indicates Bering Sea, temperature curve, whereas the purple lines show Pacific temperature curves. Grey lines show Holocene SST records to each core, which are related to the grey axis at the bottom(SO201-2-85KL: Max et al. (2012)).. For core details see Table.1. Numbers on top indicate marine isotope stages. Light blue background color indicates cold, orange warm phases.

NW Africa Eglinton (1992). Core details are stated in **Table 1**. SST values from core M23414 are derived from planktic foraminifera and represent summer temperatures (Bauch et al., 2012). Comparison of calculated SST derived from different methods is still problematic, as can be seen in diverging records from the same samples. This can be caused by diverse factors, such as different depth of habitats or seasonal production peaks (Leduc et al, 2010). Never the less, this record was chosen because the number of northern N-Atlantic alkenone SST records, with a sufficient resolution is limited. All other records are alkenone based and use the Prahl et al. (1988) calibration and do not represent summer, but annual mean temperatures.

In the deglaciation phase, the southern cores show temperature peaks which, unlike in core SO 201-2-85KL, do not reach the interglacial SST level. The temperature minima at 131 ka BP can be also identified in core MD01-2444 and ODP108-658, but it is not followed by the onset of the rising trend towards the interglacial maximum. In both cores there is a short peak and another temperature fall after the 131 ka BP temperature low. At core M23414, the temperature stays cold, with a low variability until a very strong rise of more than 9°C at 125 ka BP. In all N-Atlantic locations, the temperature at the last interglacial is delayed compared to the Bering Sea record. During other MIS 5 sub-stages all cores correlate with the general climate patterns. There is one exception, that of core ODP108-658, where high temperature variability without a clear trend is visible. The other sub-stages and the Holocene are not represented in this record. Beginning in MIS 5c, the northern SST record M23414 shows a higher variability compared to other records. This includes temperatures during the cold phases (MIS 5b, 4) reaching levels as high as during the warm stages 5c and 5a. The difference at the early Eemian between the 2 southern cores and core SO201-2-85KL is less than 3 ka. Therefore, this might also fall in the possible stratigraphic inaccuracy of core SO201-2-85KL.

Neither in the Holocene records of core M23414 nor in core MD01-2444 can the B/A thermal peak or the YD low be identified. Instead both records show a rising trend in two steps, with a steady phase at 13 ka BP. In both cores the difference between the early Holocene and the Eemian maximal temperatures is more than 2°C. The enhanced temperature during the Eemian period, compared to the HTM is also observed further to the north in a core from the South Icelandic Basin (Eynaud et al., 2004).

5.6. SST comparisons in context

The peaks in summer insolation at MIS 5c and 5a are both less intense than the MIS 5e (**see Fig.16, p. 34**). This is reflected in the temperatures in all MIS 5 SST records (except for ODP 145-882, probably due to scarce data over MIS 5e), which is an additional indicator, that insolation is the main climate driver throughout MIS 5.

Comparing differences between Holocene and Eemian SSTs of North Atlantic and North Pacific it can be observed, that all records show 1-3°C warmer temperatures during the Eemian. This temperature difference cannot be found in the Bering Sea. This discrepancy is especially important regarding core ODP 145-882, where the temperature difference between both periods is high compared to other shown records, although this location, at least after modern current pattern, is strongly influenced by water masses originating from the Bering Sea.

Similar results to those of the Bering Sea were published by van Nieuwenhove & Bauch (2008), who compared last interglacial and Holocene surface water conditions in the Norwegian Sea and found the MIS 5e climatic optimum comparable with the average Holocene. However the comparison showed also a late optimum in the last interglacial in contrast to an early one in the Holocene. The delay is explained by a weakened North Atlantic drift (Bauch et al., 2012).

Such a delay is not revealed in the Bering Sea. Five of the six shown records from Atlantic and Pacific, have delayed temperature rises towards MIS 5e compared to the Bering Sea. Partly this still may be due to stratigraphic inaccuracies, but three records have main temperature rises during the last interglacial more than 3 ka later compared to the Bering Sea. This could indicate that the glacial/interglacial transition began at least slightly earlier in the Bering Sea, which would mean that this area was more sensitive regarding the increasing insolation. Therefore, though both regions do not show increased Eemian temperatures compared to the Holocene, it does not seem probable that the Nordic Sea and the Bering Sea were parallel coupled. Otherwise one would expect a more similar development of temperature trends. However it cannot be excluded that the influence of the Arctic Ocean to Adjacent seas may have been during the last interglacial than today.

Considering other sub stages of MIS5 the Bering Sea does correlate better with the North Atlantic records, where similar to core SO201-2-85KL all stages are distinctive. However the northern North Pacific records lack in their resolution during the late MIS5, which makes comparisons more difficult.

5.7. Comparison of Holocene and Emmian sea ice condition

Max et al. (2012) published qualitative Holocene IP_{25} data taken from cores from the western Bering Sea. This data revealed a strong dynamic in annual sea ice extend, as depicted in **Figure 15**. During warm periods like HTM or B/A, no IP_{25} could be detected, indicating sea ice retreated to the shelf area. In the colder periods YD and Heinrich Event 1, IP_{25} was even detected in a core located at the southern edge of the Shirshov Ridge. In these periods, the annual maximum sea ice edge moved at least 250 km southward (Max et al., 2012).
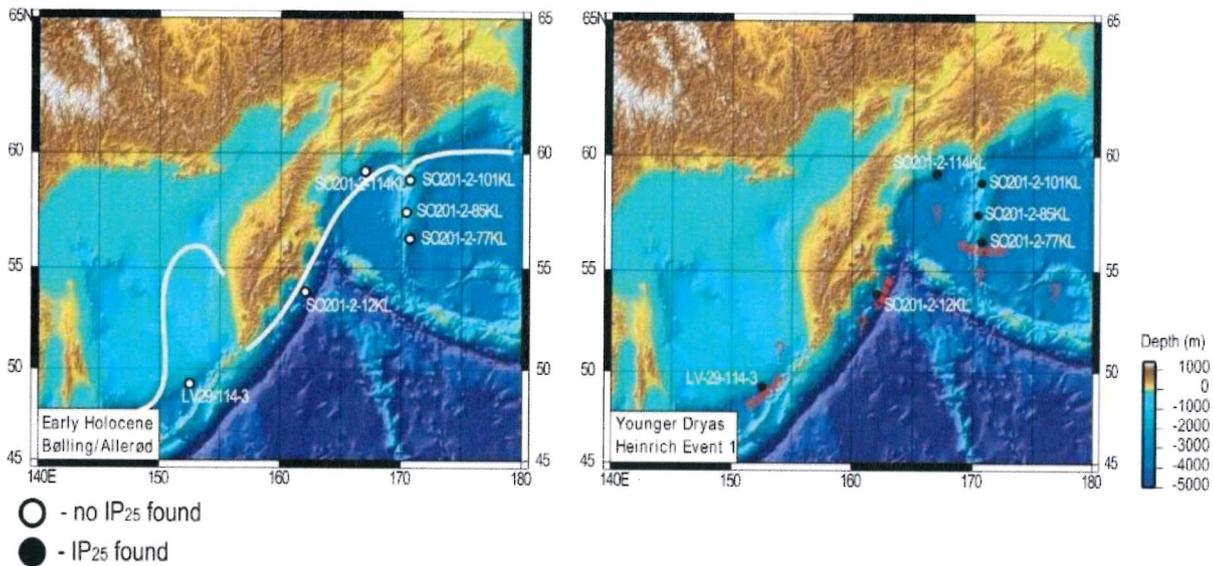
Figure 15: Sea ice extend in the Western Bering Sea and Sea of Ochotsk during early Holocene and Termination 1 (Max et al., 2012).

In general, the sea ice situation in MIS 5 seems similar. Cold phases go along with IP_{25} appearance, while MIS 5e is mostly accompanied by IP_{25} absence. Comparable to the SST development, the glacial-interglacial transition is not a simple change between a condition with sea ice and one without, but a dynamic process that involves changing a few times between both states. Due to the lack of comparable datasets from nearby sites, it is not possible to make assumptions about a possible shift of the annual maximum sea ice extend. Considering the modern genesis of sea ice in the Bering Sea, and the described situation during Younger Dryas and Heinrich 1, the sea ice is generated at the coast north of the Shirshov Ridge. Therefore, the assumed sea ice extend could be an analogue to the glacial extend as shown in **Figure 15**, reaching at least as far south as site SO201-2-85KL.

Riethdorf et al. (2012) proposed a possible perennial sea ice cover in the NW Bering Sea during termination II, which might explain existence of exceptionally coarse material during this

period in core 85. This would be correspond to parallel suggested patterns from the Sea of Ochotsk (Nürnberg et al., 2011). During wide parts of late MIS 6 and glacial termination II, alkenones could be detected in more than minimal quantities, which strongly suggest at least ice-free summer seasons. The coexistence of IP_{25} in this period indicates seasonal sea ice occurrence. A thick lasting sea ice cover would lead to an absence of IP_{25}, and alkenones. Still the question of the origin from off coarse material remains.

5.8. Sea Ice and winter insolation

Sea ice occurrence and summer SST as plotted in **Figure 12 (p. 26)** seem to contradict samples, in which high temperatures do coincide with ice occurrence as well as samples with low SST and no IP_{25}. These anomalies identify changes in the inner annual temperature dynamics. A possible explanation for this contradiction may be given by the comparison of Eemian winter and summer insolation, as done in **Figure 16**. The high summer insolation at 115 ka BP is accompanied by very low winter insolation, while the low summer insolation at 130 ka BP correlates to a maxima in winter insolation. According to the IP_{25} data the summer insolation is not a critical factor concerning Bering Sea ice extend.
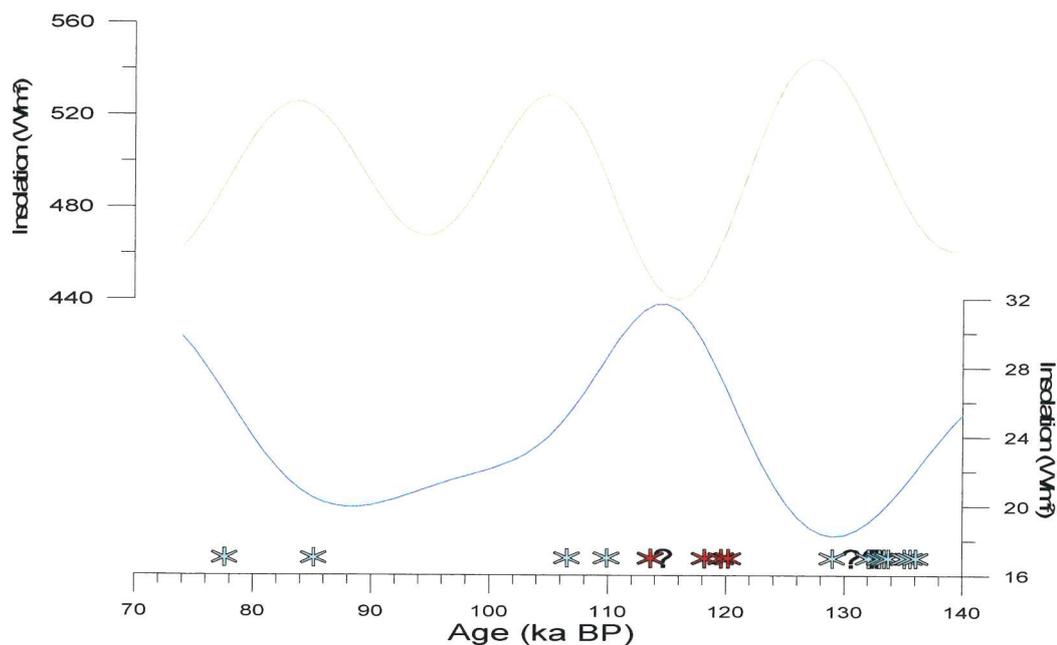
Figure 16: June (green) and December insolation at 60°N plotted against time

Symbols at the bottom indicate IP25 occurrence (blue stars), absence (red stars), or quantities near detection limits. Data source: Berger & Loutre (1991)

6. Conclusion

The results of this thesis can be summarized shortly in the following statements:

- Eemian peak SSTs, were not higher than Holocene maximum temperatures

- Development of surface temperature and sea ice occurrence in the Bering Sea during glacial termination II show many similarities to glacial termination I.

- The SST reconstruction from the Bering Sea does not reflect a thermal dipole relation between North Atlantic and Bering Sea during glacial termination II or MIS 5.

Temperature Comparison

In the geographic setting and discussion, evidence was shown that insolation was probably one of the main climate drivers throughout MIS 5. Therefore, the high insolation during MIS 5e would be expected to cause a warmer climate in the Northern hemisphere when compared to early Holocene times. With respect to sea surface temperature this period of warm climate is observed in the North Atlantic as well as in the open North Pacific, but not in the Bering Sea. This implies that there was obviously an additional cooling factor during MIS 5e in the Western Bering Sea. Such a cooling factor could be an enhanced transport of relatively cold air or water masses into the Bering Sea, or an increased outflow, or decreased inflow of relatively warm water. A similar phenomenon, with equal temperatures during MIS 5e and the early Holocene, is visible in the Northern Sea and is explained there with a weakening of the North Atlantic Drift, decreasing the input of warm water masses (Bauch et al., 2012).

During the Eemian temperature high, the summer temperature is enhanced severely in Siberia. Kienast et al. (2011) also showed that the Siberian coast line was shifted northwards in this period, despite the high sea level. Both factors may have led to a stronger Siberian high, which enhanced the southward transport of cold arctic air masses over the Western Bering Sea, during summer.

Another possible cooling factor could be a change of the Bering Sea current system. Although it is very unlikely that the Bering Strait led cold surface water masses southwards, it may still

have influenced the Bering Sea SST. Due to a higher Eemian sea level, the Bering Strait was wider, which amplified the outflow of relatively warm surface water from the Bering Sea to the Arctic Ocean. This resulted in an enhanced energy transfer to the Arctic Ocean, slowing down the warming of the surface water within the Bering Sea. On the other hand, the rising sea level affected also the gateways in the Aleutian Arc at the southern edge of the Bering Sea, increasing the amount of incoming warm surface water from the Pacific. To evaluate the dimension and importance of each of those factors, further scientific work in this direction is necessary. The most promising approach is probably climate modelling. It should focus on heat transfer through the Bering Strait and atmospheric exchange between the Arctic Ocean and the Bering Sea, in order to be able to explain the somewhat unexpected temperatures similar to the Holocene maximum despite the increased insolation.

Parallels regarding glacial termination

The comparison of Holocene and Eemian SST from Atlantic and Pacific cores, respectively, revealed that at most core locations the final temperature rise towards the interglacial maximum evolved parallel in both periods. The glacial terminations however, showed differences in most cases. In core SO201-2-85KL both glacial terminations look very much alike. A period of cold is ended by a short warm period, followed by a steep temperature decrease, which prevailed for a short period and was in turn followed by the final rise in temperature. The short warm period has about the same temperature as the interglacial high while the following cool phase is accompanied by temperatures at the glacial level.

These steps are similar to glacial termination I (Max eta l., 2012), supported by IP_{25} data showing sea ice occurrence during cold and no ice in warm phases. The main difference between the two terminations lies in their relation to summer insolation. The observed shift in temperature patterns, when both records are aligned according to their insolation curves, could not be observed in other records. This is probably due to stratigraphic uncertainties. Another explanation would be an accelerated deglaciation mechanism due to steeper increase in insolation. Considering all other Eemian SST curves presented in this thesis, this seems very unlikely and should have been visible also in other records. To improve the stratigraphic correlation, comparison of the data of this thesis to other MIS5 cores from the Bering Sea may be helpful. However, the closely located cores SO201-2-77KL and SO201-2-101KL probably won't be able to improve depth-age correlation, as their age model so far is, amongst other

factors, based on correlation on color b* to core SO201-2-85KL (Riethdorf et al., 2012). A suggested perennial sea ice cover (Riethdorf et al., 2012) during MIS6, which would explain very coarse ice rafted debris, seems rather unlikely, considering the new data of this thesis. The major argument against such a lasting ice cover is the presence of alkenones, which could be confirmed throughout the investigated core parts representing MIS 6.

Over regional teleconnections

The results of this thesis neither indicated an Atlantic-Pacific temperature seesaw, nor an in phase temperature trend relation between both oceans. The Eemian SST development from the Bering Sea, especially the equality to Holocene maximum temperatures, shows different behaviour compared to the Pacific, as well as to the Atlantic Ocean. Additional the uncertainty regarding the stratigraphy over MIS5e in core SO201-2-85KL, visible from comparison to the Holocene record, prevent a reliable comparison to temperature trends from other regions during high dynamic phases, like glacial termination II. To clarify, if North Atlantic and North Pacific had parallels in temperature trends during MIS 6/5e transition, like it has been suggested for glacial termination I (Max et al., 2012), would need further SST data preferable also from the northwestern North Pacific. However, the lack of alkenones and TOC during MIS 5d and during late glacial termination II, fits within the suggested seesaw regarding meridional overturning circulation, indicating NPIW formation (Horikawa et al., 2010). This also confirms model results suggesting a meridional overturning circulation seesaw during phases when the Bering Strait is closed (Hu et al., 2012).

Acknowledgments

Table of Figures

References

Armand, L.K. and Leventer, A., 2010. Paleo sea ice distribution and reconstruction derived from the geologic record. In: D.N. Thomas and G.S. Dieckmann (Eds.), Sea ice. Oxford, Wiley-Blackwell, 469-529.

Axford, Y., Briner, J.P., Francis, D.R., Miller, G.H., Walker, I.R. and Wolfe, A.P., 2011. Chironomids record terrestrial temperature changes throughout Arctic interglacials of the past 200,000 yr. Geological Society of America Bulletin, 7-8: 1275-1287.

Barker, S., Cacho, I., Benway, H. and Tachikawa, K., 2005. Planktonic foraminiferal Mg/Ca as a proxy for past oceanic temperatures: a methodological overview and data compilation for the Last Glacial Maximum. Quaternary Science Reviews; Multiproxy Approach for the Reconstruction of the Glacial Ocean surface, 7: 821-834.

Bauch, H.A., Kandiano, E.S. and Helmke, J.P., 2012. Contrasting ocean changes between the subpolar and polar North Atlantic during the past 135 ka. Geophysical Research Letters, 11: n/a-n/a.

Belt, S.T., MassÃ©, G., Rowland, S.J., Poulin, M., Michel, C. and LeBlanc, B., 2007. A novel chemical fossil of palaeo sea ice: IP25. Organic Geochemistry, 1: 16-27.

Berger, A. and Loutre, M.F., 1991. Insolation values for the climate of the last 10 million years. Quaternary Science Reviews, 4: 297-317.

Brassell, S.C., Eglinton, G., Marlowe, I.T., Pflaumann, U. and Sarnthein, M., 1986. Molecular stratigraphy: a new tool for climatic assessment. Nature, 6058: 129-133.

Caissie, B.E., Brigham-Grette, J., Lawrence, K.T., Herbert, T.D. and Cook, M.S., 2010. Last Glacial Maximum to Holocene sea surface conditions at Umnak Plateau, Bering Sea, as inferred from diatom, alkenone, and stable isotope records. Paleoceanography, 1: PA1206.

CAPE Last Interglacial Project members, 2006. Last Interglacial Arctic warmth confirms polar amplification of climate change. Quaternary Science Reviews, 13–14: 1383-1400.

Debret, M., Desmet, M., Balsam, W., Copard, Y., Francus, P. and Laj, C., 2006. Spectrophotometer analysis of Holocene sediments from an anoxic fjord: Saanich Inlet, British Columbia, Canada. Marine Geology, 1–2: 15-28.

Dullo,W., Baranov,B. and van den Bogaard,C. eds., 2009. FS Sonne Fahrtbericht / Cruise Report SO201-2 KALMAR: Kurile-Kamchatka and ALeutian MARginal Sea-Island Arc Systems: Geodynamic and Climate Interaction in Space and Time, Busan/Korea - Tomakomai/Japan, 30.08. - 08.10.2009. Kiel: .

Eglinton, G., Bradshaw, S., Resell, A., Sarnthein, M., Pflaumann, U. and Tiedemann, R., 1992. Molecular record of secular sea surface temperature changes on 100-year timescales for glacial terminations I, II and IV. Nature, 6368: 423-426.

EU Climate Change Expert Group 'EG Science', 2008. The 2°C Target Information reference document. Background on Impacts, EmissionPathways, Mitigation Options and Costs.

Eynaud, F., Turon, J.L. and Duprat, J., 2004. Comparison of the Holocene and Eemian palaeoenvironments in the South Icelandic Basin: dinoflagellate cysts as proxies for the North Atlantic surface circulation. Review of palaeobotany and palynology, 1–2: 55-79.

Fütterer, D.K., 2005. The solid phase of marine sediments. In: H.D. Schulz and M. Zabel (Eds.), Marine geochemistry. Berlin, Springer, 1-25.

Harada, N., Shin, K.H., Murata, A., Uchida, M. and Nakatani, T., 2003. Characteristics of alkenones synthesized by a bloom of *Emiliania huxleyi* in the Bering Sea. Geochimica et Cosmochimica Acta, 8: 1507-1519.

Hensen, C., Zabel, M. and Schulz, H.D., 2005. Benthic cycling of oxygen, nitrogen and phosphorus. In: H.D. Schulz and M. Zabel (Eds.), Marine geochemistry. Berlin, Springer, 207-240.

Horikawa, K., Asahara, Y., Yamamoto, K. and Okazaki, Y., 2010. Intermediate water formation in the Bering Sea during glacial periods: Evidence from neodymium isotope ratios. Geology, 5: 435-438.

Hu, A., Meehl, G.A., Han, W., Abe-Ouchi, A., Morrill, C., Okazaki, Y. and Chikamoto, M.O., 2012. The Pacific-Atlantic seesaw and the Bering Strait. Geophysical Research Letters, 3: L03702.

Katsuki, K. and Takahashi, K., 2005. Diatoms as paleoenvironmental proxies for seasonal productivity, sea-ice and surface circulation in the Bering Sea during the late Quaternary. Deep-Sea Research Part II, 16-18: 2110-2130.

Kiefer, T. and Kienast, M., 2005. Patterns of deglacial warming in the Pacific Ocean: a review with emphasis on the time interval of Heinrich event 1. Quaternary Science Reviews, 7–9: 1063-1081.

Kienast, F., Wetterich, S., Kuzmina, S., Schirrmeister, L., Andreev, A.A., Tarasov, P., Nazarova, L., Kossler, A., Frolova, L. and Kunitsky, V.V., 2011. Paleontological records indicate the occurrence of open woodlands in a dry inland climate at the present-day Arctic coast in western Beringia during the Last Interglacial. Quaternary Science Reviews, 17–18: 2134-2159.

Kim, J., Rimbu, N., Lorenz, S.J., Lohmann, G., Nam, S., Schouten, S., Rühlemann, C. and Schneider, R.R., 2004. North Pacific and North Atlantic sea-surface temperature variability during the Holocene. Quaternary Science Reviews, 20–22: 2141-2154.

Kopp, R.E., Simons, F.J., Mitrovica, J.X., Maloof, A.C. and Oppenheimer, M., 2009. Probabilistic assessment of sea level during the last interglacial stage. Nature, 7275: 863-867.

Kukla, G.J., Bender, M.L., de Beaulieu, J., Bond, G., Broecker, W.S., Cleveringa, P., Gavin, J.E., Herbert, T.D., Imbrie, J., Jouzel, J., Keigwin, L.D., Knudsen, K., McManus, J.F., Merkt, J., Muhs, D.R., Müller, H., Poore, R.Z., Porter, S.C., Seret, G., Shackleton, N.J., Turner, C., Tzedakis, P.C. and Winograd, I.J., 2002. Last Interglacial Climates. Quaternary Research, 1: 2-13.

Leduc, G., Schneider, R., Kim, J.-. and Lohmann, G., 2010. Holocene and Eemian sea surface temperature trends as revealed by alkenone and Mg/Ca paleothermometry. Quaternary Science Reviews, 7–8: 989-1004.

Lisiecki, L.E. and Raymo, M.E., 2005. A Pliocene-Pleistocene stack of 57 globally distributed benthic ?18O records. Paleoceanography, 1: - PA1003.

Locarnini, R.A., Mishonov, A.V., Antonov, J.I., Boyer, T.P., Garcia, H.E., Baranova, O.K., Zweng, M.M. and Johnson, D.R., 2010. World Ocean Atlas 2009, Volume 1: Temperature.. S. LEVITUS ed., Washington, D.C.: U.S. Government Printing Office.

Mangelsdorf, K., Güntner, U. and Rullkötter, J., 2000. Climatic and oceanographic variations on the California continental margin during the last 160 kyr. Organic Geochemistry, 9: 829-846.

Martínez-Garcia, A., Rosell-Melé, A., McClymont, E.L., Gersonde, R. and Haug, G.H., 2010. Subpolar Link to the Emergence of the Modern Equatorial Pacific Cold Tongue. Science, 5985: 1550-1553.

Martrat, B., Grimalt, J.O., Shackleton, N.J., de Abreu, L., Hutterli, M.A. and Stocker, T.F., 2007. Four Climate Cycles of Recurring Deep and Surface Water Destabilizations on the Iberian Margin. Science, 5837: 502-507.

Max, L., Riethdorf, J., Tiedemann, R., Smirnova, M., Lembke-Jene, L., Fahl, K., Nürnberg, D., Matul, A. and Mollenhauer, G., 2012. Sea surface temperature variability and sea-ice extent in the subarctic northwest Pacific during the past 15,000 years Paleoceanography, 3:.

Müller, J., Wagner, A., Fahl, K., Stein, R., Prange, M. and Lohmann, G., 2011. Towards quantitative sea ice reconstructions in the northern North Atlantic: A combined biomarker and numerical modelling approach. Earth and Planetary Science Letters, 3: 137-148.

Müller, P.J., Kirst, G., Ruhland, G., von Storch, I. and Rosell-Melé, A., 1998. Calibration of the alkenone paleo-temperature index UK'37 based on core-tops from the eastern South Atlantic and the global ocean (60°N-60°S). Geochimica et Cosmochimica Acta, 10: 1757-1772.

NEEM community members, 2013. Eemian interglacial reconstructed from a Greenland folded ice core. Nature, 7433: 489-494.

Niebauer, H.J., Bond, N.A., Yakunin, L.P. and Plotnikov, V.V., 1999. An Update on the Climatology and Sea Ice of the Bering Sea. In: T.R. Loughlin and K. Ohtani (Eds.), Dynamics of the Bering Sea: A Summary of Phys-ical, Chemical, and Biological Characteristics, and a Synopsis of Research on the Bering Sea. Fairbanks, Univer-sity of Alaska Sea Grant, 29-59.

Niebauer, H.J., 1988. Effects of El Nino-Southern Oscillation and North Pacific weather patterns on interannual variability in the subarctic Bering Sea. Journal of Geophysical Research: Oceans, C5: 5051-5068.

Nürnberg, D., Dethleff, D., Tiedemann, R., Kaiser, A. and Gorbarenko, S.A., 2011. Okhotsk Sea ice coverage and Kamchatka glaciation over the last 350 ka — Evidence from ice-rafted debris and planktonic δ18O. Palaeo-geography, Palaeoclimatology, Palaeoecology, 3–4: 191-205.

Otto-Bliesner, B.L., Marshall, S.J., Overpeck, J.T., Miller, G.H., Hu, A. and CAPE Last Interglacial Project members, 2006. Simulating Arctic Climate Warmth and Icefield Retreat in the Last Interglaciation. Science, 5768: 1751-1753.

Overpeck, J.T., Otto-Bliesner, B.L., Miller, G.H., Muhs, D.R., Alley, R.B. and Kiehl, J.T., 2006. Paleoclimatic Evidence for Future Ice-Sheet Instability and Rapid Sea-Level Rise. Science, 5768: 1747-1750.

Prahl, F.G., Mix, A.C. and Sparrow, M.A., 2006. Alkenone paleothermometry: Biological lessons from marine sediment records off western South America. Geochimica et Cosmochimica Acta, 1: 101-117.

Prahl, F.G., Muehlhausen, L.A. and Zahnle, D.L., 1988. Further evaluation of long-chain alkenones as indicators of paleoceanographic conditions. Geochimica et Cosmochimica Acta, 9: 2303-2310.

Rasmussen, S.O., Andersen, K.K., Svensson, A.M., Steffensen, J.P., Vinther, B.M., Clausen, H.B., Siggaard-Andersen, M.-., Johnsen, S.J., Larsen, L.B., Dahl-Jensen, D., Bigler, M., Röthlisberger, R., Fischer, H., Goto-Azuma, K., Hansson, M.E. and Ruth, U., 2006. A new Greenland ice core chronology for the last glacial termi-nation. Journal of Geophysical Research: Atmospheres, D6: - D06102.

Riethdorf, J.-., Nürnberg, D., Max, L., Tiedemann, R., Gorbarenko, S.A. and Malakhov, M.I., 2012. Millennial-scale variability of marine productivity and terrigenous matter supply in the western Bering Sea over the past 180 kyr. Climate of the Past Discussions, 6: 6135-6198.

Rohling, E.J., Grant, K., Hemleben, C., Siddall, M., Hoogakker, B.A.A., Bolshaw, M. and Kucera, M., 2008. High rates of sea-level rise during the last interglacial period. Nature Geosci, 1: 38-42.

Rullkötter, J., 2005. Organic matter: The driving force for early diagenesis. In: H.D. Schulz and M. Zabel (Eds.), Marine geochemistry. Berlin, Springer, 125-168.

Shackleton, N.J., Sánchez-Goñi, M.F., Pailler, D. and Lancelot, Y., 2003. Marine Isotope Substage 5e and the Eemian Interglacial. Global and Planetary Change, 3: 151-155.

Sikes, E.L., Volkman, J.K., Robertson, L.G. and Pichon, J., 1997. Alkenones and alkenes in surface waters and sediments of the Southern Ocean: Implications for paleotemperature estimation in polar regions. Geochimica et Cosmochimica Acta, 7: 1495-1505.

Stabeno, P.J., Schumacher, J.D. and Ohtani, K., 1999. The physical oceanography of the Bering Sea. In: T.R. Loughlin and K. Ohtani (Eds.), Dynamics of the Bering Sea: A Summary of Physical, Chemical, and Biological Characteristics, and a Synopsis of Research on the Bering Sea. Fairbanks, University of Alaska Sea Grant, 1-28.

Tanaka, S. and Takahashi, K., 2005. Late Quaternary paleoceanographic changes in the Bering Sea and the western subarctic Pacific based on radiolarian assemblages. Deep Sea Research Part II: Topical Studies in Oceanography, 16–18: 2131-2149.

Ternois, Y., Kawamura, K., Ohkouchi, N. and Keigwin, L., 2000. Alkenone sea surface temperature in the Okhotsk Sea for the last 15 kyr. Geochemical Journal, 34: 283-293.

Van Nieuwenhove, N. and Bauch, H.A., 2008. Last interglacial (MIS 5e) surface water conditions at the Vøring Plateau (Norwegian Sea), based on dinoflagellate cysts. Polar Research, 2: 175-186.

Zhao, M., Huang, C., Wang, C. and Wei, G., 2006. A millennial-scale $U37K'$ sea-surface temperature record from the South China Sea (8°N) over the last 150 kyr: Monsoon and sea-level influence. Palaeogeography, Palaeoclimatology, Palaeoecology, 1–2: 39-55.

Appendix

Age (ka BP)	Depth (cm bsf)	Sea surface temperature calibrations			IP$_{25}$	remarks
		Prahl et al. (1988)	Müller et al. (1998)	Sikes et al. (1997)		
77.6	873	2.2	2.2	5.2	+	
78.6	883	5.8	5.8	8.4		
80.9	903	6.1	6.1	8.6		
83.1	923	6.9	6.9	9.3		
84.2	933	6.6	6.6	9.1		
85.2	943	4.6	4.5	7.3	+	
85.9	953		no alkenones			
86.7	963		no alkenones			
88.6	983		concentration too low			2 x GC
90.0	993	6.1	6.1	8.6		
91.3	1003		no alkenones			
92.6	1013		concentration too low			2 x GC
93.9	1023	9.1	9.2	11.3		2 x GC
95.3	1033	6.6	6.7	9.1		
97.8	1052	7.0	7.1	9.5		2 x GC
100.9	1076		no alkenones			
103.2	1093		no alkenones			
103.6	1096		no alkenones			
104.1	1100		no alkenones			
105.0	1111		no alkenones			
106.6	1131	6.6	6.7	9.1	+	
107.8	1146	5.0	5.0	7.7		
108.5	1156		no alkenones			
109.0	1163		no alkenones			
109.2	1166		concentration too low			2 x GC
109.9	1176	4.5	4.5	7.2	+	2 x GC
110.5	1183	4.8	4.8	7.4		2 x GC
110.8	1186		concentration too low			2 x GC
111.5	1193		concentration too low			2 x GC
111.9	1196		concentration too low			2 x GC
112.6	1203		concentration too low			2 x GC
112.9	1206		concentration too low			2 x GC
113.6	1213	6.4	6.5	8.9	-	
113.8	1215		concentration too low			2 x GC
113.9	1216	9.6	9.8	11.8		
114.7	1223	3.0	2.9	5.8	?	
116.0	1233		concentration too low			2 x columned
116.5	1236		concentration too low			2 x columned
117.6	1243		concentration too low			2 x columned
118.2	1246	6.0	6.0	8.5	-	
119.6	1253	4.6	4.6	7.3	-	
120.2	1256	6.3	6.4	8.8	-	2 x GC
121.6	1263	6.0	6.0	8.5		
122.2	1266	5.6	5.6	8.2		
123.6	1273	6.1	6.1	8.7		
124.2	1276	5.6	5.6	8.2		
125.8	1283	6.4	6.4	8.9		
126.3	1285	8.4	8.5	10.7		

Age (ka BP)	Depth (cm bsf)	Sea surface temperature calibrations			IP_{25}	remarks
		Prahl et al. (1988)	Müller et al. (1998)	Sikes et al. (1997)		
126.3	1285	8.4	8.5	10.7		
126.5	1286	6.7	6.7	9.1		
128.3	1293	6.7	6.8	9.2		
128.8	1295	8.1	8.2	10.4		
129.0	1296	8.0	8.1	10.4	+	
130.3	1303		no alkenones			
130.5	1305		concentration too low			2 x GC
130.6	1306	4.9	4.9	7.6	?	
131.0	1310	4.6	4.6	7.3		
131.30	1313	4.7	4.7	7.4		
131.60	1316		concentration too low			2 x GC
132.07	1321	4.3	4.3	7.0	+	
132.13	1322	10.6	10.7	12.6		
132.20	1323	6.5	6.6	9.0		
132.40	1326	7.8	7.9	10.2	?	
132.80	1332	3.8	3.8	6.6	?	
132.87	1333	4.9	4.9	7.6		
133.00	1335	5.5	5.5	8.1	+	
133.07	1336	5.4	5.5	8.0		
133.40	1341	3.4	3.3	6.2	+	
133.47	1342	3.9	3.8	6.6		
133.53	1343	5.3	5.3	8.0		
133.73	1346	5.8	5.8	8.4	+	
134.07	1351	5.3	5.3	7.9		
134.40	1356	4.7	4.6	7.3		
134.73	1361	4.2	4.2	7.0		
135.10	1366	4.1	4.1	6.8	+	
135.58	1371	7.0	7.0	9.4	+	
136.07	1376	4.2	4.1	6.9	+	
137.04	1386	5.1	5.1	7.7		
137.52	1391	4.7	4.7	7.4		
138.49	1401	4.8	4.8	7.5		

Table 2: Results of SST calculation derived from $U^{K'}_{37}$, and IP_{25} analyses. 2 x GC indicates samples with low alkenone concentration, which were measured a second time in the GC with less hexane. '+' indicates IP_{25} in sample, '-' indicates no IP_{25} in sample and '?' indicates IP_{25} near detection limit.